LETTER

https://doi.org/10.1038/s41586-019-1069-7

TMK1–mediated auxin signalling regulates differential growth of the apical hook

Min Cao[1,2,3,5], Rong Chen[1,5], Pan Li[1,2,3,5], Yongqiang Yu[1,2], Rui Zheng[1,2,3], Danfeng Ge[1,2,3], Wei Zheng[2], Xuhui Wang[2], Yangtao Gu[2], Zuzana Gelová[4], Jiří Friml[4], Heng Zhang[1], Renyi Liu[2], Jun He[1,2] & Tongda Xu[2]*

The plant hormone auxin has crucial roles in almost all aspects of plant growth and development. Concentrations of auxin vary across different tissues, mediating distinct developmental outcomes and contributing to the functional diversity of auxin. However, the mechanisms that underlie these activities are poorly understood. Here we identify an auxin signalling mechanism, which acts in parallel to the canonical auxin pathway based on the transport inhibitor response1 (TIR1) and other auxin receptor F-box (AFB) family proteins (TIR1/AFB receptors)[1,2], that translates levels of cellular auxin to mediate differential growth during apical-hook development. This signalling mechanism operates at the concave side of the apical hook, and involves auxin-mediated C-terminal cleavage of transmembrane kinase 1 (TMK1). The cytosolic and nucleus-translocated C terminus of TMK1 specifically interacts with and phosphorylates two non-canonical transcriptional repressors of the auxin or indole-3-acetic acid (Aux/IAA) family (IAA32 and IAA34), thereby regulating ARF transcription factors. In contrast to the degradation of Aux/IAA transcriptional repressors in the canonical pathway, the newly identified mechanism stabilizes the non-canonical IAA32 and IAA34 transcriptional repressors to regulate gene expression and ultimately inhibit growth. The auxin–TMK1 signalling pathway originates at the cell surface, is triggered by high levels of auxin and shares a partially overlapping set of transcription factors with the TIR1/AFB signalling pathway. This allows distinct interpretations of different concentrations of cellular auxin, and thus enables this versatile signalling molecule to mediate complex developmental outcomes.

In both animals and plants, cellular concentrations of signalling molecules affect their biological roles: distinct activities over a range of concentrations contribute to the functional diversity of given signalling molecules[3]. In plants, auxin has repeatedly been discussed as having a morphogen-like property that appears to form gradients across tissues, and to act in a concentration-dependent manner[4,5]. Differential auxin distribution is mediated by local biosynthesis[6] and directional intercellular transport[7], but the mechanisms by which the auxin gradient mediates various developmental outputs remain largely unclear. Apical-hook development in dicotyledonous plants represents a classical model that involves differential auxin concentrations. Apical-hook development in *Arabidopsis thaliana* comprises three sequential steps: formation, maintenance and opening[8,9]. Auxin asymmetrically accumulates at the concave side of the hook during the formation stage[10] (Extended Data Fig. 1a–c), which correlates with the inhibition of cell elongation, and differential growth alongside the hook leads to the bending of the hook[9,11,12].

To obtain insight into the mechanism by which auxin regulates apical-hook development, we analysed *yuc1-D* and *wei8-3 tar2-1* (*WEI8* is also known as *TAA1*) *A. thaliana* mutants that display increased[13] and decreased[14,15] auxin biosynthesis, respectively. Both mutants abolished the differential growth of the apical hook, but in different ways: auxin overproduction was accompanied by growth inhibition at the convex side of the hook, whereas decreased auxin correlated with the release of growth inhibition at the concave side of the hook (Extended Data Fig. 1d–g). Although auxin typically promotes cell elongation in shoots[16], in the context of the apical hook the local accumulation of auxin is correlated with growth inhibition.

To uncover the mechanism that underlies this particular growth inhibition, we analysed *Arabidopsis* mutants that are defective in auxin signalling. Notably, the mutant that is defective in TMK1—which is implicated in auxin signalling at the cell surface[17]—also displayed disrupted development of the apical hook (Fig. 1a, b, Extended Data Fig. 1h). The growth inhibition at the concave side of the hook was released in the *tmk1* mutant, and the resulting phenotype in the maintenance stage was rescued by the *TMK1* genomic fragment (Fig. 1c, d). Furthermore, whereas three *tmk1* mutant alleles (*tmk1-1*, *tmk1-2* and *tmk1-3*) had a similar phenotype in the maintenance stage (Extended Data Fig. 2a–d), other *tmk* mutants (*tmk2-1*, *tmk3-1* and *tmk4-1*) did not show any obvious defect (Extended Data Fig. 2e, f). The apical-hook defect in the maintenance stage in the *tmk1* mutant is different from the formation defects in auxin-transport mutants[9,18]. The defect of the *tmk1* mutant was similar to that of the *wei8-3 tar2-1* double mutant (Extended Data Fig. 1d–g), however, whereas treatment with exogenous auxin (specifically, indole-3-acetic acid (IAA)) rescued the apical-hook defect of the *wei8-3 tar2-1* double mutant, auxin was ineffective in rescuing the phenotype of the *tmk1-1* mutant (Extended Data Fig. 2g, h). These observations reveal that TMK1 participates in auxin-mediated growth inhibition during apical-hook development—presumably not by regulating auxin transport or levels of auxin. We therefore focused on the hypothesis that TMK1 functions in downstream auxin-signal transduction.

To gain additional insights into the role of TMK1 in auxin-mediated growth inhibition during apical-hook development, we analysed the in vivo distribution pattern of TMK1 protein by immunostaining, using anti-TMK1 C terminus ($TMK1_{C\text{-terminus}}$) antibody (Extended Data Fig. 2b). We observed a cytosolic and nuclear distribution of TMK1 specifically at the concave side of the apical hook during the maintenance stage—but not earlier (during the formation stage) or later (during the opening stage) (Fig. 1e, f, Extended Data Fig. 3a–e). We also detected TMK1 proteins within the apical hook by western blot, and revealed a substantial amount of truncated TMK1 protein (of approximately 50 kDa in size) during the maintenance phase (Fig. 1g). Mass spectrometry analysis of the truncated TMK1 band detected peptides from the $TMK1_{C\text{-terminus}}$, which spans amino acids 511 to 942 (Extended Data Fig. 4a, b). This suggests that TMK1 is specifically cleaved and internalized at the concave side of the hook during the maintenance phase.

The spatio-temporal pattern of TMK1 cleavage correlated with asymmetric auxin accumulation in the apical hook. To test whether increased levels of auxin lead to TMK1 cleavage, we first analysed the *wei8-3 tar2-1* double mutant and found that in this mutant TMK1 cleavage was reduced (Fig. 1g, Extended Data Fig. 4c). Furthermore, the

[1]Shanghai Center for Plant Stress Biology, Center for Excellence in Molecular Plant Sciences, Chinese Academy of Sciences, Shanghai, China. [2]FAFU-UCR Joint Center, Horticulture Biology and Metabolomics Center, Haixia Institute of Science and Technology, Fujian Agriculture and Forestry University, Fuzhou, China. [3]University of Chinese Academy of Sciences, Beijing, China. [4]Institute of Science and Technology Austria, Klosterneuburg, Austria. [5]These authors contributed equally: Min Cao, Rong Chen, Pan Li. *e-mail: tdxu@sibs.ac.cn

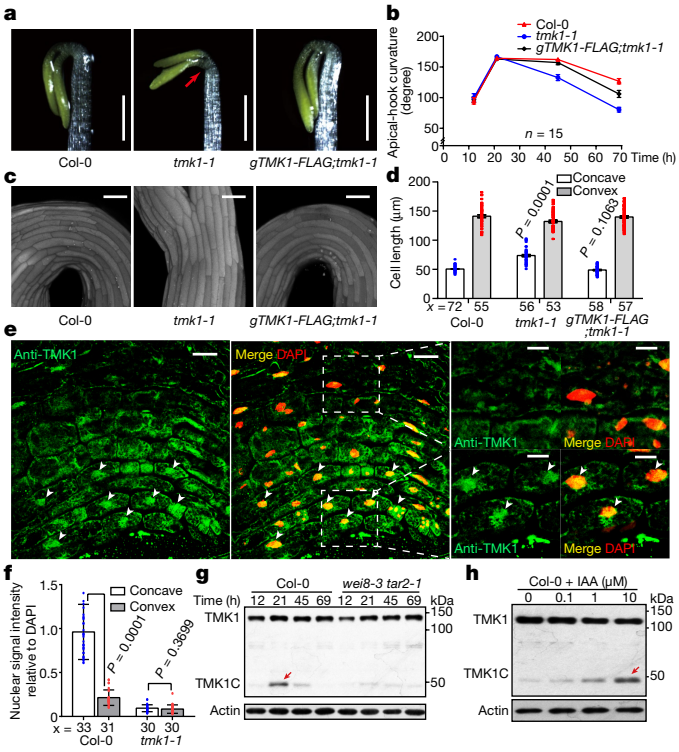

Fig. 1 | Auxin-mediated TMK1 cleavage during apical-hook maintenance. a, Images of the apical hook in Col-0, *tmk1-1* and *gTMK1-FLAG;tmk1-1* lines (representative of four out of six T3 independent lines) at the maintenance phase (45 h after germination; see time-course analysis in Extended Data Fig. 1h). **b**, Quantification of apical-hook curvature over time. $n = 15$, data are mean ± s.e.m. Throughout, n indicates the number of biologically independent seedlings. **c**, Cell elongation in the hook at the same phase (45 h after germination). **d**, Quantification of cell length. Col-0, $n = 15$; *tmk1-1*, $n = 15$; *gTMK1-FLAG;tmk1-1*, $n = 17$; x, number of cells; two-sided t-test; data are mean ± s.e.m. **e**, Immunolocalization of TMK1 protein in the apical hook (left). Magnification of concave (bottom right) and convex (top right) sides of the hook; arrowheads indicate nuclei. Green indicates TMK1 localization, red indicates DAPI. **f**, Quantification of relative nuclear signal intensity of TMK1. $n = 8$; x, cell numbers; two-sided t-test; data are mean ± s.e.m. **g**, Western blot of TMK1 proteins at different apical-hook stages in wild-type and *wei8-3 tar2-1* plants. **h**, Western blot of TMK1 proteins treated with different concentrations of auxin. Arrowheads in **g** and **h** indicate cleaved TMK1. For **g**, **h**, the same membrane was stripped and blotted with anti-actin antibodies as a loading control. Three biological repeats (**g**, **h**). Dots show data distribution. Scale bars, 500 μm (**a**), 50 μm (**c**), 20 μm (**e** left and middle), 10 μm (**e** right). TMK1C, $TMK1_{C\text{-terminus}}$.

auxin biosynthesis inhibitor yucasin[19] also reduced cleavage of TMK1, whereas the effect was reversed when the auxin levels were restored (Extended Data Fig. 4d, e). We further confirmed that TMK1 cleavage was promoted by auxin in a dose-dependent manner (Fig. 1h, Extended Data Fig. 4f). Notably, this cleavage does not appear to require canonical TIR1 auxin signalling[1], because the TIR1 pathway antagonist phenylethyl-2-one (PEO)-IAA[20] did not have an obvious effect on auxin-promoted TMK1 cleavage (Extended Data Fig. 4g, h). Similarly, ethylene—another major regulator of apical-hook development[8,18]—did not obviously alter TMK1 cleavage, nor did the *tmk1* mutant show an altered response to treatment with the ethylene precursor 1-aminocyclopropane-1-carboxylic acid (ACC) (Extended Data Fig. 4i, j). These observations suggest that local auxin accumulation at the concave side of the hook leads to specific cleavage of the $TMK1_{C\text{-terminus}}$.

To link auxin-mediated TMK1 cleavage to local growth inhibition at the concave side of the apical hook, we expressed $TMK1_{C\text{-terminus}}$–GFP driven by the *TMK1* promoter in *tmk1-1*. The majority of $TMK1_{C\text{-terminus}}$–GFP accumulated in the cytosol and nucleus (Extended data Fig. 5a), similar to the intracellular localization of TMK1 (Fig. 1e). Importantly, *pTMK1-*$TMK1_{C\text{-terminus}}$*-GFP* could partially complement the *tmk1-1* apical-hook development defect (Extended Data Fig. 5b, c), which suggests that auxin-mediated TMK1 cleavage at the concave side of the hook is part of the mechanism of auxin-mediated growth inhibition.

To address the question of how auxin-triggered TMK1 cleavage inhibits growth at the concave side of the hook, we identified potential interaction partners of $TMK1_{C\text{-terminus}}$ using a yeast two-hybrid screen. Among the $TMK1_{C\text{-terminus}}$ candidate interactors, we focused on the IAA32 protein, because it is a member of the Aux/IAA transcription repressors that are typically associated with the TIR1/AFB auxin signalling pathway[21]. An unbiased yeast two-hybrid assay for all combinations of the 29 Aux/IAA proteins and the C terminus of all four TMK family members revealed that only $TMK1_{C\text{-terminus}}$ and the C terminus of TMK2 ($TMK2_{C\text{-terminus}}$) specifically interact with IAA32 and IAA34, and not with other IAA proteins (Fig. 2a, Extended Data Fig. 6a, b)—however, TMK2 is not expressed in the apical hook[22]. Using pull-down and co-immunoprecipitation assays, we confirmed the specific interaction of $TMK1_{C\text{-terminus}}$ with IAA32 and IAA34, but not with other IAA proteins (Extended Data Fig. 6d, e). Phylogenetic tree analyses revealed that IAA32 and IAA34 belong to the same sub-family of non-canonical IAA proteins (Extended Data Fig. 6c) that lack domain II[23] (Fig. 2b), which is required for interaction with the TIR1 receptor. Therefore, IAA32 and IAA34 did not interact with TIR1 with or without auxin, whereas auxin promotes interaction between TIR1 and canonical IAA proteins[24,25] (Fig. 2c). This suggests that TMK1 and TIR1 may interact with different subsets of Aux/IAA transcriptional repressors, and therefore facilitate auxin signalling by distinct mechanisms.

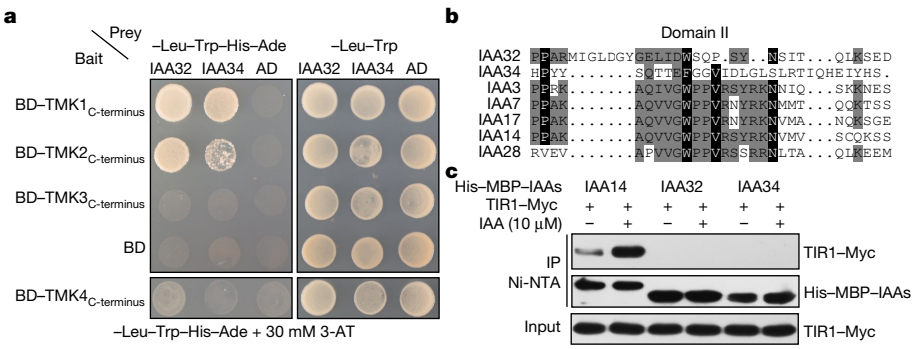

Fig. 2 | $TMK1_{C\text{-terminus}}$ specifically interacts with IAA32 and IAA34. a, Yeast two-hybrid assay of C terminus of TMK proteins, and IAA32 and IAA34. At 30 mM 3-amino-1,2,4-triazole (3-AT) inhibits auto-activation of the C terminus of TMK4 ($TMK4_{C\text{-terminus}}$) in yeast. Three biological repeats. Ade, adenine; BD, DNA-binding domain; AD, activation domain. **b**, Sequence alignment of domain II in Aux/IAA proteins, performed using the T-coffee program. **c**, Pull-down assay between plant-extracted TIR1–Myc and *Escherichia coli*-purified 6×His–MBP–IAA recombinant proteins, with or without auxin (10 μM IAA). Three biological repeats.

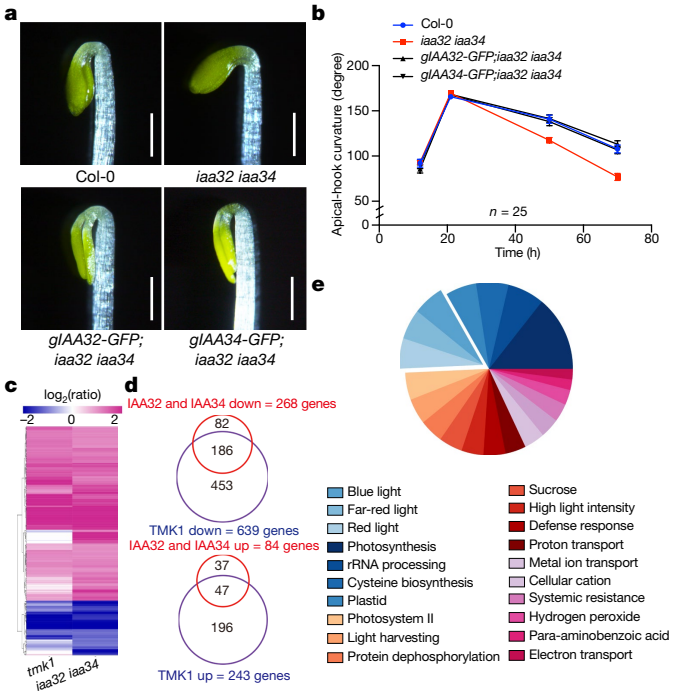

Fig. 3 | IAA32 and IAA34 regulate apical-hook maintenance, similar to TMK1. a, Apical-hook phenotypes in Col-0, *iaa32 iaa34*, *gIAA32-GFP;iaa32 iaa34* (two T3 lines) and *gIAA34-GFP;iaa32 iaa34* (two T3 lines), as described in Fig. 1a (see time-course analysis in Extended Data Fig. 8c). Scale bars, 50 μm. **b**, Quantification of apical-hook curvature over time. $n = 25$ biologically independent seedlings; data are mean ± s.e.m. **c**, RNA sequencing analysis in the apical hook of *tmk1* and *iaa32 iaa34* mutants compared to Col-0. Hierarchical clustering analysis of TMK1, IAA32 and IAA34 target genes. **d**, Venn diagrams showing overlap of genes regulated by TMK1 and genes regulated by IAA32 and IAA34. Up, upregulated; down, downregulated. **e**, Gene Ontology analysis of upregulated genes in both *tmk1* and *iaa32 iaa34* mutants.

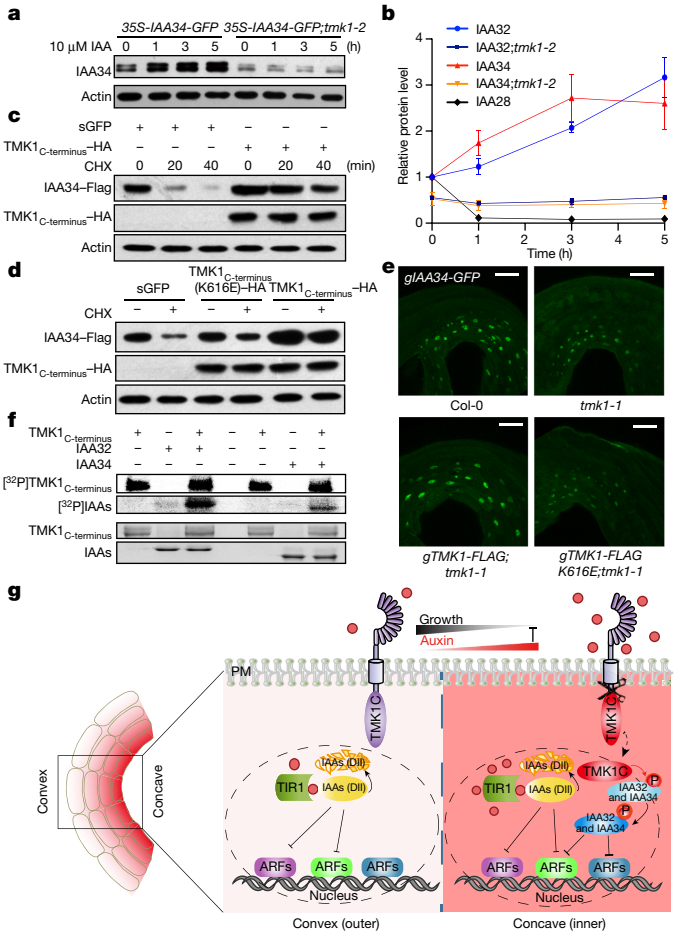

Fig. 4 | An auxin–TMK1–IAA32 and –IAA34 relay for apical-hook maintenance. a, Western blot analysis of etiolated *35S-IAA34-GFP* in either wild-type or *tmk1* plants treated with auxin for indicated periods of time. **b**, Quantification of relative levels of IAA protein in auxin treatment. $n = 3$ biological repeats, data are mean ± s.e.m. **c**, The protein stability of IAA34, with or without co-expression of 35S–$TMK1_{C\text{-terminus}}$–HA. Treatment with cycloheximide (CHX) for indicated time periods. 35S–superfolder (s)GFP as control. Three biological repeats. **d**, The protein stability of IAA34 co-expressed with $TMK1_{C\text{-terminus}}$ or $TMK1(K616E)_{C\text{-terminus}}$ mutant in protoplast, with or without treatment with CHX for 40 min. Three biological repeats. For **a**, **c** and **d**, the same membrane was stripped and blotted with anti-actin antibodies as a loading control. **e**, Confocal microscopy of IAA34–GFP protein in apical hook of the *tmk1* mutant with *gTMK1-FLAG* or *gTMK1(K616E)-FLAG*. Scale bars, 50 μm. Three biological repeats. **f**, In vitro kinase assays of $TMK1_{C\text{-terminus}}$ on IAA32 and IAA34 proteins. Two biological repeats. **g**, Proposed model of auxin–TMK1–IAA32 and IAA34 signalling in apical-hook development. A comparison with the TIR1-dependent pathway is shown. DII, domain II; PM, plasma membrane; TMK1C, $TMK1_{C\text{-terminus}}$.

To gain insight into the biological roles of these non-canonical Aux/IAA transcriptional repressors that are targeted by $TMK1_{C\text{-terminus}}$, we used *IAA32*- and *IAA34*-promoter-driven β-glucuronidase (GUS) (*pIAA32-GUS* and *pIAA34-GUS*) and IAA32–GFP and IAA34–GFP (*gIAA32-GFP* and *gIAA34-GFP*) to visualize their expression patterns and subcellular localization. Notably, both IAA32 and IAA34 were detected at the apical hook (Extended Data Fig. 7a–c) in a spatial and temporal pattern that was similar to both auxin distribution and TMK1 cleavage. IAA32 and IAA34 also showed a pattern of subcellular localization that overlapped with $TMK1_{C\text{-terminus}}$ in the cytosol and nucleus (Extended Data Fig. 7d). To address the function of IAA32 and IAA34 in apical-hook development, we generated *iaa32* and *iaa34* mutants using CRISPR–Cas9 technology (Extended Data Fig. 8a, b). Although the single-knockout mutants did not show an obvious phenotype (data not shown), the *iaa32 iaa34* double mutant exhibited an apical-hook maintenance defect similar to that seen in *tmk1*, which was complemented by the genomic fragment of *IAA32* and *IAA34* fused with GFP; this confirms that IAA32 and IAA34 have a redundant function in the regulation apical-hook maintenance (Fig. 3a, b, Extended Data Fig. 8c). Accordingly, IAA32 and IAA34 were also required for growth inhibition at the concave side of the apical hook (Extended Data Fig. 8d, e).

The interaction of $TMK1_{C\text{-terminus}}$ with the Aux/IAA transcriptional regulators suggests that this pathway regulates gene transcription. Therefore, we compared the apical-hook transcriptome of *tmk1* and *iaa32 iaa34* mutants to that of the wild type. The majority of genes were upregulated in both *tmk1* and *iaa32 iaa34* mutants (Fig. 3c, d). Notably, 69.4% (186 out of 268) of upregulated genes and 56.0% (47 out of 84) of downregulated genes in the *iaa32 iaa34* mutant overlapped with those in *tmk1* mutant (Fig. 3d), and about half of these co-regulated genes contained auxin-response elements[26] (Extended Data Fig. 9a). The co-regulated genes were mainly related to auxin responses, such as SAUR family genes or light signalling related to apical-hook opening[27] (Fig. 3e). Furthermore, IAA32 and IAA34 interacted with a subset of ARF transcription factors (Extended Data Fig. 9b) and could suppress the activity of both ARF2 and ARF7[28] (Extended Data Fig. 9c, d). This further confirms that the IAA32 and IAA34 repressors that interact with $TMK1_{C\text{-terminus}}$ regulate gene transcription by regulating ARF activity.

Canonical Aux/IAA repressors are targeted by TIR1, which ultimately leads to their proteasome-dependent degradation[29]. IAA32 and IAA34 are targeted by $TMK1_{C\text{-terminus}}$ but not TIR1, which suggests that they possess a distinct regulatory mechanism. In contrast to the auxin-mediated degradation of canonical Aux/IAA repressors, treatment of *35S-IAA32-GFP* and *35S-IAA34-GFP* seedlings with

auxin promoted an accumulation of IAA32 and IAA34 proteins over time (Fig. 4a, b, Extended Data Fig. 10a, b). In the *tmk1-2* mutant, the amount of IAA32 and IAA34 protein strongly decreased, and auxin was entirely ineffective in promoting the accumulation of these proteins (Fig. 4a, b, Extended Data Fig. 10a, b). We also found that, as with TMK1 cleavage, PEO-IAA did not affect the auxin-mediated accumulation of IAA32 and IAA34 proteins: this is consistent with IAA32 and IAA34 not being a target of TIR1 (Extended Data Fig. 10c). This suggests that auxin stabilizes IAA32 and IAA34 proteins via TMK1, which represents a regulatory mechanism that is opposite to that of the classic TIR1-dependent mechanism. Nevertheless, the TIR1 pathway regulated *IAA32* and *IAA34* transcription (Extended Data Fig. 10d). These observations imply that TMK1- and TIR1-based mechanisms regulate IAA32 and IAA34 at the post-transcriptional and transcriptional levels, respectively, which coordinates the asymmetric accumulation of the IAA32 and IAA34 proteins that regulate gene expression and inhibit growth at the concave side of the apical hook.

Furthermore, co-expression of $TMK1_{C\text{-terminus}}$ with IAA32 and IAA34 in protoplasts markedly promoted the accumulation of IAA32 and IAA34. Treatment with cycloheximide, a protein synthesis inhibitor, revealed that IAA32 and IAA34 were unstable proteins that could be stabilized by $TMK1_{C\text{-terminus}}$ (Fig. 4c, Extended Data Fig. 10e, f). Because $TMK1_{C\text{-terminus}}$ contains the kinase domain, we used a mutated $TMK1_{C\text{-terminus}}$ variant ($TMK1(K616E)_{C\text{-terminus}}$) in which the C-terminal kinase domain was inactivated, and showed that kinase activity is essential for the stabilization of the IAA32 and IAA34 proteins (Fig. 4d, Extended Data Fig. 10g). Consistently, the *TMK1* promoter-driven TMK1(K616E) could not rescue the apical-hook phenotype or stability of the IAA32 and IAA34 proteins in the *tmk1* mutant (Fig. 4e, Extended Data Fig. 10h–j), which suggests that $TMK1_{C\text{-terminus}}$ acts via phosphorylation. Indeed, using an in vitro kinase assay, we detected the direct phosphorylation of IAA32 and IAA34 proteins by $TMK1_{C\text{-terminus}}$ (Fig. 4f). Taken together, these data suggest that $TMK1_{C\text{-terminus}}$ phosphorylates IAA32 and IAA34 through its kinase activity, which increases the stability of the IAA32 and IAA34 proteins.

Our observations uncover a transcriptional auxin signalling pathway that originates at the cell surface, and through which local auxin accumulation modulates asymmetric growth during apical-hook development (Fig. 4g). Given the complex developmental defects of multiple *tmk* mutants and the range of potential $TMK1_{C\text{-terminus}}$ interactors we identified, it would be worthwhile to understand the full repertoire of the developmental processes—beyond those of the apical hook—that are controlled by this newly identified auxin signalling pathway.

Online content

Any methods, additional references, Nature Research reporting summaries, source data, statements of data availability and associated accession codes are available at https://doi.org/10.1038/s41586-019-1069-7.

Received: 16 March 2018; Accepted: 27 February 2019;
Published online 3 April 2019.

1. Salehin, M., Bagchi, R. & Estelle, M. SCFTIR1/AFB-based auxin perception: mechanism and role in plant growth and development. *Plant Cell* **27**, 9–19 (2015).
2. Weijers, D. & Wagner, D. Transcriptional responses to the auxin hormone. *Annu. Rev. Plant Biol.* **67**, 539–574 (2016).
3. Kicheva, A., Bollenbach, T., Wartlick, O., Jülicher, F. & Gonzalez-Gaitan, M. Investigating the principles of morphogen gradient formation: from tissues to cells. *Curr. Opin. Genet. Dev.* **22**, 527–532 (2012).
4. Bargmann, B. O. et al. A map of cell type-specific auxin responses. *Mol. Syst. Biol.* **9**, 688 (2013).
5. Friml, J. et al. AtPIN4 mediates sink-driven auxin gradients and root patterning in *Arabidopsis*. *Cell* **108**, 661–673 (2002).
6. Zhao, Y. Essential roles of local auxin biosynthesis in plant development and in adaptation to environmental changes. *Annu. Rev. Plant Biol.* **69**, 417–435 (2018).
7. Adamowski, M. & Friml, J. PIN-dependent auxin transport: action, regulation, and evolution. *Plant Cell* **27**, 20–32 (2015).
8. Raz, V. & Ecker, J. R. Regulation of differential growth in the apical hook of *Arabidopsis*. *Development* **126**, 3661–3668 (1999).
9. Zádníková, P. et al. Role of PIN-mediated auxin efflux in apical hook development of *Arabidopsis thaliana*. *Development* **137**, 607–617 (2010).
10. Liao, C. Y. et al. Reporters for sensitive and quantitative measurement of auxin response. *Nat. Methods* **12**, 207–210, 2, 210 (2015).
11. Li, H., Johnson, P., Stepanova, A., Alonso, J. M. & Ecker, J. R. Convergence of signaling pathways in the control of differential cell growth in *Arabidopsis*. *Dev. Cell* **7**, 193–204 (2004).
12. Žádníková, P. et al. A model of differential growth-guided apical hook formation in plants. *Plant Cell* **28**, 2464–2477 (2016).
13. Zhao, Y. et al. A role for flavin monooxygenase-like enzymes in auxin biosynthesis. *Science* **291**, 306–309 (2001).
14. Stepanova, A. N. et al. TAA1-mediated auxin biosynthesis is essential for hormone crosstalk and plant development. *Cell* **133**, 177–191 (2008).
15. Tao, Y. et al. Rapid synthesis of auxin via a new tryptophan-dependent pathway is required for shade avoidance in plants. *Cell* **133**, 164–176 (2008).
16. Fendrych, M., Leung, J. & Friml, J. TIR1/AFB-Aux/IAA auxin perception mediates rapid cell wall acidification and growth of *Arabidopsis* hypocotyls. *eLife* **5**, e19048 (2016).
17. Xu, T. et al. Cell surface ABP1–TMK auxin-sensing complex activates ROP GTPase signaling. *Science* **343**, 1025–1028 (2014).
18. Vandenbussche, F. et al. The auxin influx carriers AUX1 and LAX3 are involved in auxin-ethylene interactions during apical hook development in *Arabidopsis thaliana* seedlings. *Development* **137**, 597–606 (2010).
19. Nishimura, T. et al. Yucasin is a potent inhibitor of YUCCA, a key enzyme in auxin biosynthesis. *Plant J.* **77**, 352–366 (2014).
20. Hayashi, K. et al. Small-molecule agonists and antagonists of F-box protein-substrate interactions in auxin perception and signaling. *Proc. Natl Acad. Sci. USA* **105**, 5632–5637 (2008).
21. Overvoorde, P. J. et al. Functional genomic analysis of the AUXIN/INDOLE-3-ACETIC ACID gene family members in *Arabidopsis thaliana*. *Plant Cell* **17**, 3282–3300 (2005).
22. Wu, Y. et al. Genome-wide expression pattern analyses of the *Arabidopsis* leucine-rich repeat receptor-like kinases. *Mol. Plant* **9**, 289–300 (2016).
23. Ramos, J. A., Zenser, N., Leyser, O. & Callis, J. Rapid degradation of auxin/indoleacetic acid proteins requires conserved amino acids of domain II and is proteasome dependent. *Plant Cell* **13**, 2349–2360 (2001).
24. Dharmasiri, N., Dharmasiri, S. & Estelle, M. The F-box protein TIR1 is an auxin receptor. *Nature* **435**, 441–445 (2005).
25. Kepinski, S. & Leyser, O. The *Arabidopsis* F-box protein TIR1 is an auxin receptor. *Nature* **435**, 446–451 (2005).
26. Ulmasov, T., Hagen, G. & Guilfoyle, T. J. ARF1, a transcription factor that binds to auxin response elements. *Science* **276**, 1865–1868 (1997).
27. Mazzella, M. A., Casal, J. J., Muschietti, J. P. & Fox, A. R. Hormonal networks involved in apical hook development in darkness and their response to light. *Front. Plant Sci.* **5**, 52 (2014).
28. Bielach, A. et al. Spatiotemporal regulation of lateral root organogenesis in *Arabidopsis* by cytokinin. *Plant Cell* **24**, 3967–3981 (2012).
29. Gray, W. M., Kepinski, S., Rouse, D., Leyser, O. & Estelle, M. Auxin regulates SCF^{TIR1}-dependent degradation of AUX/IAA proteins. *Nature* **414**, 271–276 (2001).

Acknowledgements We thank J. Sheen and Z. Yang for critical comments and suggestions; J. Du for providing the pDu vector. This work was supported by National Key R&D Program of China (2016YFA0503200) and National Natural Science Foundation of China (Grant 31422008), CAU State Key Laboratory of Plant Physiology and Biochemistry open funds, start-up funds from PSC and FAFU to T.X. and the European Union's Horizon 2020 program (ERC grant agreement no. 742985) to J.F.

Reviewer information *Nature* thanks Dolf Weijers and the other anonymous reviewer(s) for their contribution to the peer review of this work.

Author contributions T.X., M.C. and R.C. initiated the project and designed the experiments; M.C., R.C. and P.L. carried out most of the experiments; J.H., W.Z. and Z.G. did TMK1 immunolocalization; Y.Y. and R.Z. conducted protoplast and yeast two-hybrid assays; X.W. and Z.G. analysed the apical-hook phenotype; Y.G. did most of the protein purifications; H.Z. conducted the whole-genome and RNA sequencing; D.G. and R.L. analysed the sequencing data; T.X., M.C., R.C. and J.F. wrote the manuscript.

Competing interests The authors declare no competing interests.

Additional information
Extended data is available for this paper at https://doi.org/10.1038/s41586-019-1069-7.
Supplementary information is available for this paper at https://doi.org/10.1038/s41586-019-1069-7.
Reprints and permissions information is available at http://www.nature.com/reprints.
Correspondence and requests for materials should be addressed to T.X.
Publisher's note: Springer Nature remains neutral with regard to jurisdictional claims in published maps and institutional affiliations.

METHODS

No statistical methods were used to predetermine sample size. The experiments were randomized and investigators were blinded to allocation for phenotype experiments (but not biochemistry experiments) and outcome assessment.

Plant materials and growth conditions. All plant materials were grown in a plant growth chamber (PERVICAL AR-66L3) with continuous darkness at 22 °C, unless otherwise indicated. Col-0 was used as wild type. *tmk1-1* (SALK_016360), *tmk1-2* (SAIL_812_G09), *tmk1-3* (SALK_008771), *tmk2-1* (SAIL_1242_H07), *tmk3-1* (SALK_129759) and *tmk4-1* (GABI_348E01) in a Col-0 background were used for phenotypic analysis. The *iaa32* and *iaa34* single mutants were generated by CRISPR–Cas9 technology[30]. Cas9 insertion in the mutants was removed at the T3 generation. The *iaa32 iaa34* double mutant, generated by crossing, was homozygous-negative for Cas9 at the T3 generation. Genomic sequencing was performed in the *iaa32 iaa34* mutant. To generate TMK1 transgenic plants, the *TMK1* sequence (including the 3.5-kb promoter, genomic coding region and 1 kb of 3′ untranslated region) was amplified and inserted into a pDONR-Zeo vector. A Flag tag was added to the C terminus of TMK by ligation (pDONR-gTMK1), and the sequence was inserted into the pGWB501 destination vector, using the LR reaction. pGWB501-gTMK1-Flag was transformed to complement *tmk1-1*, and six T3-generation homozygous lines were used for analysis. To generate the *pTMK1-TMK1*$_{C\text{-}terminus}$*-GFP* transgenic line, a sequence including a 3.5-kb promoter and the genomic coding region (amino acids 505–942) of TMK1 was amplified together with GFP, and inserted into pGWB501 vector as described above. pTMK1-TMK1$_{C\text{-}terminus}$-GFP was transformed to complement *tmk1-1* at the T3 generation with three individual lines. To generate the *pIAA-GUS* transgenic plant, 2-kb promoter regions of IAA32 and IAA34 were amplified, inserted into the pGWB533 vector and used to transformed Col-0 (eight T2-generation heterozygous lines for both *pIAA32-GUS* and *pIAA34-GUS*). To generate *gIAA32-GFP* and *gIAA34-GFP* transgenic plants, sequences that included a 2-kb promoter and the genomic coding regions of IAA32 and IAA34 were amplified, inserted into the pGWB504 vector, and used to transform Col-0 (12 T2-generation *gIAA32-GFP* and 11 T2-generation *gIAA34-GFP* heterozygous lines) plants. One of the four T3 individual homozygous lines was crossed with *tmk1-1* to generate the *gIAA32-GFP;tmk1-1* and *gIAA34-GFP;tmk1-1* homozygous lines. To create the *gIAA32-GFP* and *gIAA34-GFP* complementation transgenic plants, the constructs described above were transformed into *iaa32 iaa34* to generate three independent *gIAA32-GFP;iaa32 iaa34* and *gIAA34-GFP;iaa32 iaa34* T3 homozygous lines. For *35S-IAA34-GFP* and *35S-IAA34-GFP* transgenic plants, the IAA32–GFP coding region was amplified and inserted into pCAMBIA1300-35S; the IAA34 coding region was amplified and inserted into pGWB505 vector, and both constructs were transformed into Col-0 to generate *35S-IAA32-GFP* and *35S-IAA34-GFP* T3 homozygous lines. One of the three T3 individual homozygous lines was crossed with *tmk1-2* to generate *35S-IAA32-GFP;tmk1-2* and *35S-IAA34-GFP;tmk1-2* homozygous lines; *tmk1-1* would have caused a *35S* silencing problem. The sequences of all primers used in transgenic plant generation are listed in Supplementary Table 1.

Apical-hook phenotype analysis and epidermal cell length measurement. The apical-hook phenotype was analysed at different stages of development in plants grown in darkness. Images of the apical hooks were taken using a Leica M205FA stereoscope at the time points indicated. For real-time analysis of apical-hook development by treatment with ACC, seedlings were grown vertically at 1/2 MS phytagel (4.2 g/l, Sigma cat. no. P8169) containing medium with or without 10 μM ACC. Apical-hook development was recorded at 1-h intervals for 9 days at 22 °C with an infrared light source (850-nm LED) by a spectrum-enhanced digital camera (EOS Canon t5i, 400DH with built-in clear wideband-multicoated filter, equipped with a standard 18–55-mm f3.5–5.6 lens and standard accessories) operated by the EOS utility software. Angles (defined as 180° minus the angle between the tangential of the apical part and the axis of the lower part of the hypocotyl) were measured by ImageJ software. The outline of epidermal cells at the apical hook was imaged through auto-fluorescence (excitation wavelength 405 nm, emission wavelength 450–550 nm), captured by a Leica SP8 confocal microscope (Leica TCS SP8 X) with a 40× water objective lens. Epidermal cell length was measured by ImageJ software after 3D reconstruction.

TMK1$_{C\text{-}terminus}$ antibody generation. TMK1$_{C\text{-}terminus}$ antibody was generated by ABclonal Biotechnology. In brief, the C terminus of TMK1 (amino acid 780–942) was cloned into pET28a vector. The recombinant protein was expressed in *E. coli* Rosetta (DE3) by 0.8 mM IPTG induction, and purified from inclusion bodies. Purified proteins were injected into rabbit as antigens. Antibodies were purified from immunized rabbit serum. The specificity of the TMK1$_{C\text{-}terminus}$ antibody was tested by western blot and immunostaining in the *tmk1* mutant. (1:2,000 dilution for western blot; 1:500 dilution for immunostaining).

Immunostaining of TMK1 in apical hook. The whole-mount immune-localization procedure was performed as previously described[31], with some modifications. In brief, seedlings were fixed with 4% paraformaldehyde in 1 × MTSB buffer (stock solution 2× MTSB: 15 g PIPES, 1.90 g EGTA, 1.22 g $MgSO_4{\cdot}7\ H_2O$ and 2.5 g KOH are dissolved in a total of 500 ml water at pH 7.0 (adjusted with KOH)) supplemented with 0.1% Triton in a 3-cm culture dish. The seedlings were transferred to microscope slides, and covered by a large cover glass, frozen in liquid nitrogen for approximately 10 s, and thawed at room temperature (this was repeated one more time if necessary). The cell walls were digested with digestion solutions (0.2% driselase (Sigma cat. no. D9515) and 0.15% macerozyme (Yakult Pharmaceutical Industry, LOT 160805-01) in 2 mM MES, pH5.0). The seedlings were transferred to membrane permeabilization solution (3% IGEPAL C630, 10% DMSO in 1× MTSB) and then incubated in blocking buffer (1× MTSB with 2% BSA (Sigma cat. no. D9515)) for 2 h. Samples were incubated with primary antibody (anti-TMK1$_{C\text{-}terminus}$, 1:500) overnight at 4 °C, washed 5 times with 1× MTSB washing buffer, and incubated with the secondary antibody solution (Dylight488 Goat anti Rabbit IgG, Invitrogen, cat. no. 35553) with 1:1,000 dilution and washed 5 times with washing buffer. The seedlings were then incubated in 1:1,000-diluted DAPI for half an hour at room temperature, and washed 3 times and kept in antifade solution.

Fluorescence imaging analysis. GFP and DyLight 488 signals were detected using a Leica SP8 confocal microscope (Leica TCS SP8 X, excitation 489 nm; emission 500–550 nm) with HyD Gating (1.5–10 ns) to diminish auto-fluorescence. DAPI was detected using the DAPI channel (excitation 405 nm; emission 410–490 nm). The intensity of fluorescence signals was calculated by ImageJ after conversion to a 16-bit grey figure. To analyse the correlation between the relative intensity of TMK1$_{C\text{-}terminus}$ immunofluorescence and DAPI in representative cells, the fluorescence intensity was calculated by ImageJ and normalized by the maximum intensity at 255. The position across the cell was normalized from 0 to 1 as shown in Extended Data Fig. 3.

For R2D2 imaging capture, Venus and tdTomato signals in the hook region were detected by a Leica SP8 confocal microscope (Leica TCS SP8 X, Venus: excitation 515 nm; emission 525–549 nm; tdTomato: excitation 554 nm; emission 570–642 nm) with a 40× water objective lens. To quantify the ratio of tdTomato:Venus, an area in the nucleus of the cell of interest of approximately 10 μm^2 in size was selected using the ROI tool, and the ratio of tdTomato:Venus signal was calculated by the Calcium Imaging Calculator built into the microscope, as previously described[10].

Phytohormone and chemical treatment. For hormone response analysis, seedlings were grown on 1/2 MS medium with agar containing 0.5 μM IAA (Sigma cat. no. I2886) or 10 μM ACC (Sigma cat. no.A3903). For biochemical assays, we used 4-day-old dark-grown seedlings on a 1/2 MS plate and transferred them to 1/2 MS liquid medium containing various chemicals. For auxin treatment, seedlings were treated with different concentrations of IAA for 5 h. For yucasin and auxin treatment, seedlings were treated with DMSO or 50 μM yucasin (Sigma cat. no. 573760) for 4 h, or 50 μM yucasin for 2 h with a subsequent 2 h treatment of 10 μM IAA. For ACC treatment, seedlings were treated with 10 μM IAA or 10 μM ACC for different time courses (0 h to 5 h as shown in the figures). For PEO-IAA and IAA treatment, seedlings were treated with DMSO or 75 μM PEO-IAA for 3 h, at which point 10 μM IAA added for different lengths of time (0 h to 5 h as shown in the figures).

Mass spectrometry analysis. Total proteins were extracted from approximately 5 g of *gTMK1-GFP* transgenic plants using extraction buffer (50 mM Tris-HCl pH7.4, 150 mM NaCl, 5 mM EDTA, 1% TritonX-100 with protease inhibitor, phosphatase inhibitor and PMSF) on ice. After centrifuging at 14,000*g* for 20 min, the supernatant was collected and incubated at 4 °C with GFP-trap agarose beads (GFP-Trap_A, gta-20, ChromoTek) for 3 h. The precipitated proteins were separated by sodium dodecyl sulfate polyacrylamide gel electrophoresis (SDS–PAGE) and stained by Coomassie blue R250. TMK1$_{C\text{-}terminus}$–GFP proteins were collected from the gel according to molecular mass, and excised by trypsin as previously described[32]. Mass spectrometry analysis was performed in an Orbitrap Fusion mass spectrometer (Thermo Fisher Scientific).

Peptides were reconstituted in 0.1% formic acid and injected into a nanoAcquity ultra-performance liquid chromatograph (Waters). The peptides were trapped in a 2G-V/MT Trap symmetry C18 column (5-μm particles, 180 μm inner diameter (ID) × 20 mm length) at a flow rate of 3 μl min^{-1} for 5 min, and separated on a BEH130 C18 analytical column (1.7-μm particles, 100 μm ID × 100 mm length) at 350 nl min^{-1}. The mobile phase buffer consisted of 0.1% formic acid in ultra-pure water; the eluting buffer was 0.1% formic acid in acetonitrile and was run over a linear gradient for 65 min. The liquid chromatography system was coupled online with Orbitrap Fusion mass spectrometry (Thermo Fisher Scientific). Tandem mass spectra (MS/MS) acquisition was performed following a full mass spectrometry survey scan by Orbitrap at a resolution of 120,000 over the *m*/*z* range of 350–1,800. MS/MS measurements were performed in top-speed mode by collision-induced dissociation scans. The target values of automatic gain controls were set as 400,000 for Orbitrap mass spectrometer and 10,000 for ion-trap MS/MS detection. Dynamic exclusion was enabled for 60 s.

MS/MS data were compared against the protein sequences of TMK1 using Mascot Daemon 2.5 (Matrix Science). The precursor mass tolerance was set to 10 ppm, and MS/MS fragment tolerance was set to 0.8 Da. Peptide assignments were filtered by an ion score cut-off of 15.

Yeast two-hybrid assay. The C termini of the TMK-family genes *TMK1*, *TMK2*, *TMK3* and *TMK4* ($TMK1_{C\text{-}terminus}$, $TMK2_{C\text{-}terminus}$, $TMK3_{C\text{-}terminus}$ and $TMK4_{C\text{-}terminus}$, respectively) were cloned and inserted into pGBKT7 vector as bait. Twenty-nine genes of the Aux/IAA family were cloned from *Arabidopsis* cDNA and inserted into pGADT7 vector as prey. For the yeast two-hybrid assay between IAA and ARFs, IAA14, IAA32 and IAA34 were cloned and inserted into pGBKT7 vector as bait. To generate ARF constructs, full-length ARF genes were cloned and inserted into the entry clone vector pDONR-Zeo using the BP reaction. The fragments were recombined into pGADT7-Gateway destination vector via the LR reaction. Yeast two-hybrid assays were carried out in the Golden Yeast strain. Yeast transformation was performed using a Frozen-EZ Yeast Transformation II Kit (Zymo Research, cat. no. T2001). The transformed yeast was grown on −Leu−Trp−His−Ade medium, with or without 30 mM 3-AT.

The interaction strength of different protein pairs was measured using ONPG (Sigma, cat. no. N1127) as a substrate in yeast strain Y187, according to the manufacturer's protocol (Clontech). In brief, the relative β-galactosidase activity was calculated using optical density (OD) at 420 nm (OD_{420}) divided by OD_{600} from 3 independent clones (6-h reaction time for $TMK1_{C\text{-}terminus}$, $TMK2_{C\text{-}terminus}$ and $TMK3_{C\text{-}terminus}$, and 3-h reaction time for $TMK4_{C\text{-}terminus}$ (owing to strong self-activation)). To verify expression of the constructs, 5-OD yeast-cell pellets were lysed in 1 ml lysis buffer (0.25 M NaOH with 1% 2-mercaptoethanol) on ice for 20 min, followed by the addition of 0.16 ml of 50% TCA and incubation on ice for 20 min. The samples were centrifuged (14,000 rpm, 10 min) and pellets resuspended in 1 ml cold acetone, and re-collected by centrifuge. The air-dried pellet was then suspended in 100 μl 2× SDS sample buffer and incubated at 100 °C for 10 min, before western blot analysis. The BD–TMK C termini were detected using anti-Myc (Myc epitope tag in pGBKT7) antibody (Sino Biological, 100029-MM08) and AD–IAA proteins were detected using anti-HA–HRP (HA epitope tag in pGADT7) antibody (Sigma, cat. no. H6533). The sequences of all primers used in the yeast two-hybrid analyses are listed in Supplementary Table 1.

Transient expression in protoplast. The coding region of $TMK1_{C\text{-}terminus}$ (amino acids 505–942) was amplified from *Arabidopsis* cDNA and inserted into a transient expression vector (HBT-HA-NOS plasmid). The $TMK1_{C\text{-}terminus}$ kinase-dead (K616E mutant) plasmid was generated by site-directed mutagenesis of the HBT-$TMK1_{C\text{-}terminus}$–HA. The coding regions of IAA14, IAA32, IAA34, IAA28, ARF2 and ARF7 were amplified and then inserted into the transient expression vector (HBT-GFP-NOS and HBT-Flag-NOS plasmid). The sequences of all primers used in the protoplast assays are listed in Supplementary Table 1.

For transient transcriptional activity assays, *Arabidopsis* mesophyll protoplasts[33] (6×10^4) were transfected with a total of 30 μg DNA (HBT-IAA32/34/28-Flag, HBT-ARF2-Flag, HBT-ARF7-Flag, 35S-GUS and DR5-LUC) and incubated overnight. Protoplast samples were used to perform the luciferase activity assay, in which GUS expression was used as an internal control. Luciferase and GUS activities were calculated after reaction with their respective substrates (luciferin (Perkin Elmer, cat. no. 122796) and 4-methyl-umbelliferyl glucuronide (Sigma, cat. no. M9130)) using a BioTek Cytation 5-cell imaging multimode reader (BioTek Instruments). Protein expression was detected by western blot (anti-Flag, Abmart no. M20008L) with a loading control (anti-actin, Abmart no. M20009L).

Recombinant protein expression and purification. The coding regions of $TMK1_{C\text{-}terminus}$, IAA14, IAA32 and IAA34 were amplified and inserted into pDu vector (His–MBP tag at N terminus) to generate His–MBP-tagged proteins. The coding regions of IAA32 and IAA34 were inserted to the pET28a vector to generate His-tagged proteins. The sequences of all primers used to generate recombinant proteins are listed in Supplementary Table 1. All constructs were transformed into *E. coli* (BL21 strain) and recombinant protein expression was induced by IPTG (0.3 mM) at 18 °C for 12 h. The cells were lysed by sonication in lysis buffer (50 mM Tris-HCl pH7.4, 150 mM NaCl, 5 mM EDTA and 20 mM imidazole with 1 mM PMSF). The supernatant was incubated with Ni-NTA resin (Qiagen cat. no. 30210) and washed with wash buffer (50 mM Tris-HCl pH7.4, 150 mM NaCl, 5 mM EDTA and 20 mM imidazole) five times. The proteins were released from the beads using elution buffer (50 mM Tris-HCl pH7.4, 150 mM NaCl, and 200 mM imidazole) and concentrated using an Amicon Ultra-4 Centrifugal Filter Unit (Merck cat. no. UFC801024).

Protein extraction and western blot analyses. Five-day-old dark-grown Col-0, *35S-IAA32-GFP*, *35S-IAA34-GFP*, *35S-IAA32-GFP;tmk1-2*, *35S-IAA34-GFP;tmk1-2* and *35S-IAA28-MYC* plants were treated in the dark with individual hormones or chemicals in 1/2 MS liquid medium. For protein extraction from the apical hook, the hook region was cut and immediately frozen in liquid nitrogen. The seedlings or hook tissues were ground with liquid nitrogen and lysed directly in 2× SDS sample buffer for 15 min on ice. The proteins were detected by western blot with corresponding primary antibodies (anti-$TMK1_{C\text{-}terminus}$; anti-GFP, Santa Cruz no. sc-9996; anti-Myc, Roche no.14242000; anti-actin, Abmart no. M20009L)

For protein extracted from protoplasts, HBT-IAA32-Flag and HBT-IAA34-Flag plasmids (10 μg) were co-transformed with HBT-sGFP, HBT-$TMK1_{C\text{-}terminus}$-HA or HBT-TMK1(K616E)$_{C\text{-}terminus}$-HA plasmids (10 μg) into 200 μl (4×10^4) protoplasts. Protoplasts were incubated in WI buffer for 5 h and then treated with 100 μM CHX (Sigma, cat. no. C1988) for the indicated times. Protoplast samples were lysed directly by 2× SDS sample buffer. The proteins were detected by western blot analysis with corresponding primary antibodies (anti-HA, Abmart no. M20003L, anti-Flag, Abmart no. M20008L, anti-actin, Abmart no. M20009L). For western blot quantification, band intensity was calculated by ImageJ. The relative amount of the target protein was normalized first to the actin-band intensity, and then to the control sample (the sample amount of the negative control, or at the first time point, was standardized as 1).

Co-immunoprecipitation assay. Co-immunoprecipitation assays were performed in the *Arabidopsis* protoplast system. Fifty micrograms plasmid DNA (HBT-$TMK1_{C\text{-}terminus}$-HA, HBT-IAA14-GFP, HBT-IAA32-GFP and HBT-IAA34-GFP) was transformed or co-transformed into 1 ml (2×10^5) protoplasts and incubated in WI buffer for 6 h. The protoplasts collected were lysed in 500 μl lysis buffer (50 mM Tris-HCl pH 7.4, 75 mM NaCl, 5 mM EDTA, 0.5% TritonX-100,1× protease cocktail inhibitors). Protein extracts were incubated with GFP-Trap agarose beads at 4 °C for 3 h. The immunoprecipitated proteins were washed three times with washing buffer (50 mM Tris-HCl pH 7.4, 75 mM NaCl, 5 mM EDTA), and detected by corresponding primary antibodies (anti-GFP, Santa Cruz no. sc-9996; anti-HA, Abmart no. M20003L).

In vitro pull-down assay. His–MBP-fused IAA proteins were expressed in *E. coli* and captured by Ni-NTA resin. $TMK1_{C\text{-}terminus}$–GFP protein was extracted from *pTMK1-TMK1$_{C\text{-}terminus}$-GFP* transgenic plants using lysis buffer (50 mM Tris-HCl pH 7.4, 75 mM NaCl, 5 mM EDTA, 0.5% TritonX-100,1× protease cocktail inhibitors) and then incubated with 20 μl His–MBP–IAA14, His–MBP–IAA32 and His–MBP–IAA34 beads at 4 °C for 3 h. The beads were washed three times with washing buffer (50 mM Tris-HCl pH 7.4, 75 mM NaCl, 5 mM EDTA). Proteins were detected with the corresponding primary antibodies (anti-GFP, Santa Cruz no. sc-9996, anti-His, Abmart no. M30111L).

TIR1 binding assay. The TIR1-binding assay was performed as previously described[24]. In brief, the binding between *E. coli*-extracted, His–MBP-fused IAA14, IAA32 and IAA34 proteins and plant- extracted Myc-fused TIR1 protein was tested with or without 10 μM IAA. The proteins were detected by western blot analysis with corresponding primary antibodies (anti-Myc, Abmart no. M20002L; anti-His, Abmart no. M30111L)

In vitro kinase assay. His–MBP–$TMK1_{C\text{-}terminus}$ protein (0.5 μg), 6×His–IAA32 and 6×His–IAA34 (0.5 μg) were mixed in reaction buffer (5 mM HEPES, 10 mM $MgCl_2$, 10 mM $MnCl_2$, 1 mM DTT with 50 μM γ^{32}P ATP and 50 μM ATP). After incubation at 25 °C for 1 h, the reaction was stopped by the addition of 5× SDS–PAGE loading buffer. Radioactive signals from His–MBP–$TMK1_{C\text{-}terminus}$, 6×His–IAA32 and 6×His–IAA34 were detected by the Typhoon imaging system (GE Healthcare TYPHOON FLA 9500).

GUS staining. Two-day-old, dark-grown seedlings of *pIAA32-GUS* and *pIAA34-GUS* were used for GUS staining. The seedlings were fixed in 90% cold acetone. The remaining acetone was washed out by staining buffer without X-Gluc (5-bromo-4-chloro-3-indolyl-β-D-glucuronide) (100 mM NaH_2PO_4, 10 mM EDTA, 0.5 mM potassium ferricyanide ($(K_3Fe(CN)_6)$, 0.5 mM potassium ferrocyanide $K_4Fe(CN)_6$, 20% methanol and 0.1% Triton X-100), and stained by staining buffer with 0.5 mg/ml X-Gluc and 0.1% Triton X-100 at 37 °C in the dark for 8 h (*pIAA32-GUS*) or 14 h (*pIAA34-GUS*). After staining, the seedlings were washed and cleared with 70% ethanol for more than 24 h, before image capture using a Leica M205FA stereoscope.

Phylogenetic analysis of the IAA family. Twenty-nine *Arabidopsis thaliana* IAA protein sequences were aligned using MUSCLE[34] with default parameters. A Bayesian reconstruction of phylogeny was estimated with MrBayes (v.3.2.7)[35], using ten simultaneous independent analyses for 100,000 generations (sampling at every 100 generations) and using the JTT + I + G + F model. Posterior probability was used to assess the statistical support for each bipartition. The final Bayesian inference tree was visualized using FigTree software (http://tree.bio.ed.ac.uk/software/figtree/).

RNA sequencing and data analysis. Forty-five-hours-old Col-0, *tmk1-1* and *iaa32 iaa34* plants were used for transcriptome analysis. To isolate the apical-hook region, the hook-shaped structure without cotyledons (~2 mm long) was cut from seedlings using a blade. Total RNA was isolated from ~50 hooks per sample using TRIzol Reagent. Total RNA (1 μg) was used in library preparation with NEBNext Ultra Directional RNA Library Prep Kit for Illumina (New England BioLabs, E7420L), according to the manufacturer's instructions with nine different barcodes (triplicate biological samples). RNA sequencing was performed at the Genomics Core Facility of Shanghai Center for Plant Stress Biology. The quality

of the raw data was assessed with FastQC (http://www.bioinformatics.babraham.ac.uk/projects/fastqc/). Clean reads were obtained by removing adaptor sequences and low-quality regions with cutadapt[36] and SolexaQA[37], respectively. Clean reads were mapped to the TAIR10 genome using HISAT[38] with default parameters. Read counts of each gene were summarized by the HTSeq count[39]. Genes with low-level expression were removed; only genes with a normalized expression level of at least one count per million in at least two samples were retained for further analysis. The R package edgeR[40] was used to identify differentially expressed genes between Col-0 and *iaa32 iaa34*, as well as between Col-0 and *tmk1-1*. The significance cut-offs for differentially expressed genes were: a change in expression of at least twofold, and a false discovery rate of less than 0.05. The R packages VennDiagram and pheatmap were used to generate Venn diagrams and heat maps, respectively.

The auxin-response element TGTCTC was identified by searching the promoter regions (2,000-bp upstream region from the translation start site) of the up- or down-regulated genes in both *tmk1* and *iaa32 iaa34* mutants. The proportion of target genes was calculated in total genes common to *tmk1* and *iaa32 iaa34* mutants.

Quantitative PCR with reverse transcription. Total RNA was isolated from ~30 hooks per sample using TRIzol Reagent. Two hundred nanograms of RNA was reverse-transcribed to cDNA by M-MLV Reverse Transcriptase (Promega M170A). Primer pairs were designed with Primer 3 software. Quantitative PCR with reverse transcription was conducted with the Bio-Rad CFX96 Real-Time System, according to the manufacturer's instructions. *UBQ10* was used as an internal control. The sequences of all primers used in quantitative PCR with reverse transcription analyses are listed in Supplementary Table 1.

Statistical analysis. All box plots, bar graphs and connecting lines were generated using GraphPad Prism 7 Software. Two-sided *t*-tests or one-way analyses of variance (ANOVA) were used for statistical analysis, using GraphPad Prism 7.

Reporting summary. Further information on research design is available in the Nature Research Reporting Summary linked to this article.

Data availability

Data that support the findings of this study are available within the paper and its Supplementary Information. RNA sequencing raw data associated with Fig. 3c, d are available at the Gene Expression Omnibus under accession number GSE111716. Source Data (gels and graphs) for Figs. 1, 3, 4 and Extended Data Figs. 1–6, 8–10 are provided with the paper.

30. Yan, L. et al. High-efficiency genome editing in *Arabidopsis* using *YAO* promoter-driven CRISPR/Cas9 system. *Mol. Plant* **8**, 1820–1823 (2015).
31. Pasternak, T. et al. Protocol: an improved and universal procedure for whole-mount immunolocalization in plants. *Plant Methods* **11**, 50 (2015).
32. Uhrig, R. G., She, Y. M., Leach, C. A. & Plaxton, W. C. Regulatory monoubiquitination of phosphoenolpyruvate carboxylase in germinating castor oil seeds. *J. Biol. Chem.* **283**, 29650–29657 (2008).
33. Yoo, S. D., Cho, Y. H. & Sheen, J. *Arabidopsis* mesophyll protoplasts: a versatile cell system for transient gene expression analysis. *Nat. Protoc.* **2**, 1565–1572 (2007).
34. Edgar, R. C. MUSCLE: multiple sequence alignment with high accuracy and high throughput. *Nucleic Acids Res.* **32**, 1792–1797 (2004).
35. Ronquist, F. et al. MrBayes 3.2: efficient Bayesian phylogenetic inference and model choice across a large model space. *Syst. Biol.* **61**, 539–542 (2012).
36. Martin M. Cutadapt removes adapter sequences from high-throughput sequencing reads. *EMBnet J.* **17**, 10–12 (2011).
37. Cox, M. P., Peterson, D. A. & Biggs, P. J. SolexaQA: at-a-glance quality assessment of Illumina second-generation sequencing data. *BMC Bioinformatics* **11**, 485 (2010).
38. Kim, D., Langmead, B. & Salzberg, S. L. HISAT: a fast spliced aligner with low memory requirements. *Nat. Methods* **12**, 357–360 (2015).
39. Anders, S., Pyl, P. T. & Huber, W. HTSeq—a Python framework to work with high-throughput sequencing data. *Bioinformatics* **31**, 166–169 (2015).
40. Robinson, M. D., McCarthy, D. J. & Smyth, G. K. edgeR: a Bioconductor package for differential expression analysis of digital gene expression data. *Bioinformatics* **26**, 139–140 (2010).

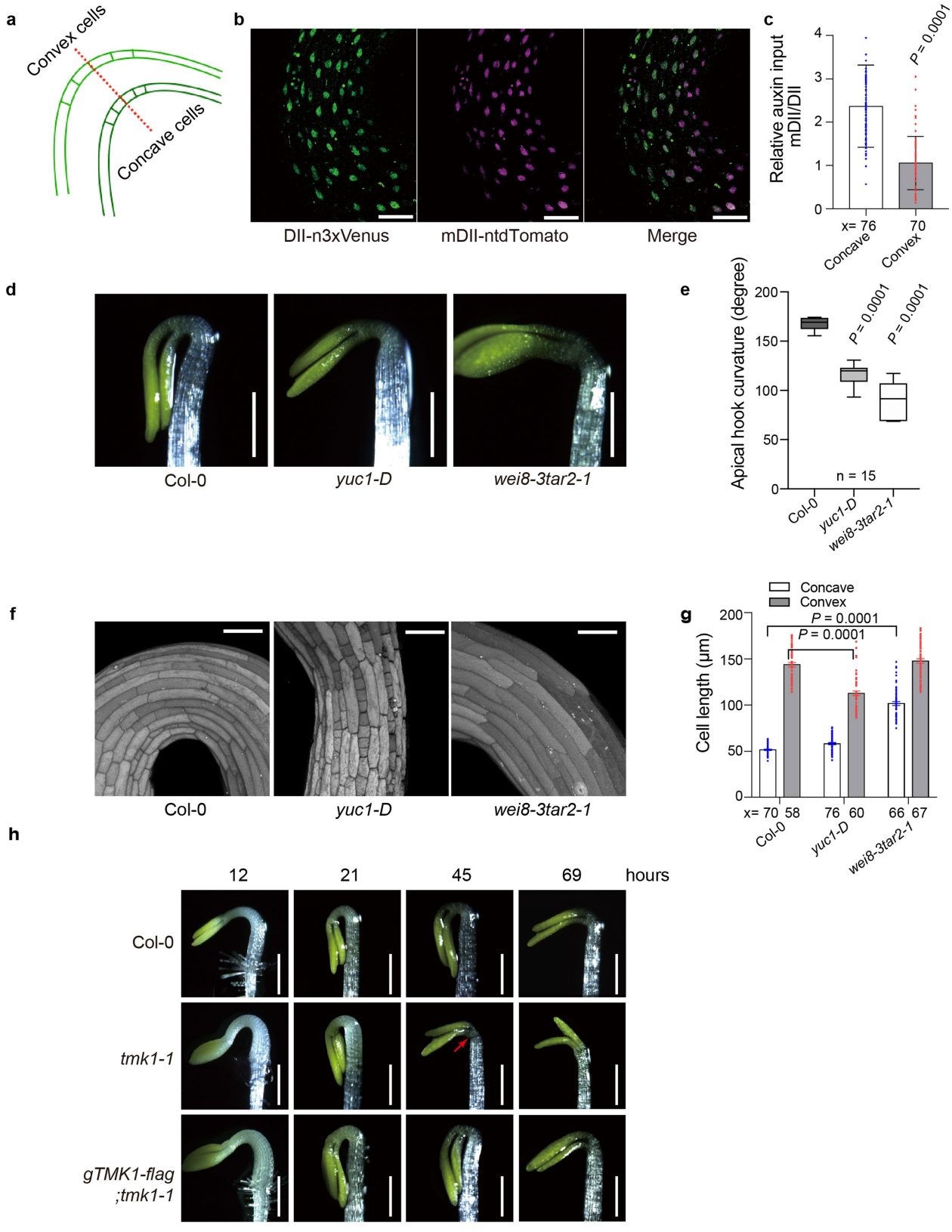

Extended Data Fig. 1 | See next page for caption.

Extended Data Fig. 1 | Disrupting the asymmetric distribution of auxin causes apical-hook development defect in *Arabidopsis*. **a**, Schematic showing cells on the concave and convex sides of the apical hook that were used for cell-length quantification. **b**, n3×Venus (green) and ntdTomato (magenta) fluorescence signal in the apical hooks of R2D2 seedlings at the maintenance stage. **c**, Quantification of the ratio of the ntdTomato to n3×Venus signals (mDII/DII, mutated domain II-to-domain II ratio) at the concave and convex sides of R2D2 apical hooks. $n = 8$; two-sided *t*-test; dots show data distribution; data are mean ± s.d. **d**, Representative images of apical hooks in Col-0, *yuc1-D* and *wei8-3 tar2-1* seedlings at 45 h after germination. **e**, Quantification of apical-hook curvature in **d**. Box plots show the first and third quartiles, split by the median and extended to minimum and maximum values. One-way ANOVA with Dunnett's multiple-comparisons test. **f**, Epidermis cell images of the apical hook in Col-0 plants, and *yuc1-D* and *wei8-3 tar2-1* mutants. **g**, Quantification of cell length at both concave and convex sides of the apical hook. Col-0 ($n = 17$), *yuc1-D* ($n = 13$), *wei8-3 tar2-1* ($n = 22$); two-sided *t*-test; dots show data distribution; data are mean ± s.e.m. **h**, Representative images of apical hooks in Col-0, *tmk1-1* and complementing *gTMK1-FLAG;tmk1-1* lines at the time points of formation (12 h), early (21 h) and late (45 h) maintenance, and opening (69 h) phases. Quantification is shown in Fig. 1b. *n* denotes the number of biologically independent seedlings; *x* denotes cell numbers. Scale bars, 50 μm (**b**,**f**); 500 μm(**d**,**h**).

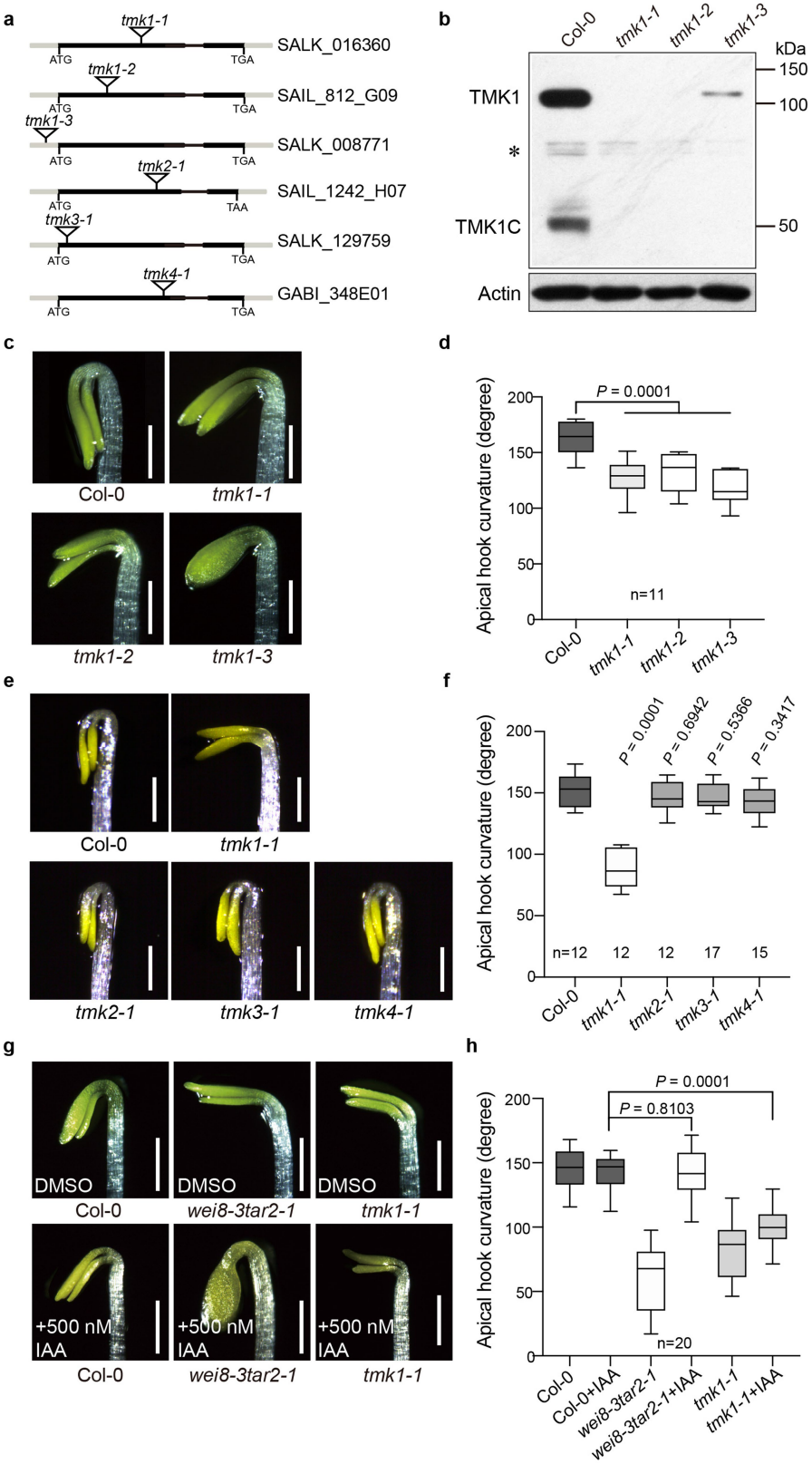

Extended Data Fig. 2 | See next page for caption.

Extended Data Fig. 2 | TMK1 specifically regulates apical-hook maintenance. a, Description of tmk transfer DNA (T-DNA) insertion mutants. Lines represent introns; black and grey boxes represent exons and untranslated regions, respectively. **b**, Western blot of the proteins extracted from the apical hook of Col-0 and different *tmk1* alleles by $TMK1_{C\text{-terminus}}$ antibody. Asterisk indicates a non-specific band. Three biological repeats. The same membrane was stripped and blotted with anti-actin antibodies as a loading control. **c**, Representative images of apical hooks in different *tmk1* alleles 45 h after germination. **d**, Quantification of apical-hook curvature in **c**. $n = 11$. **e**, Representative images of apical hooks in the mutants of different TMK family members (*tmk1-1*, *tmk2-1*, *tmk3-1* and *tmk4-1*) 48 h after germination. **f**, Quantification of apical-hook curvature in **e**. Col-0 ($n = 12$), *tmk1-1* ($n = 12$), *tmk2-1* ($n = 12$), *tmk3-1* ($n = 17$) and *tmk4-1* ($n = 15$). **g**, Representative images of apical hooks in Col-0, *wei8-3 tar2-1* and *tmk1-1* on medium supplemented with or without 0.5 μM IAA at 50 h after germination. **h**, Quantification of apical-hook curvature in **g**. $n = 20$. Box plot show the first and third quartiles, split by the median and extended to minimum and maximum values. One-way ANOVA with Dunnett's multiple-comparisons test (**d**, **f**) or two-sided *t*-test (**h**). *n* denotes the number of biologically independent seedlings. All scale bars, 500 μm.).

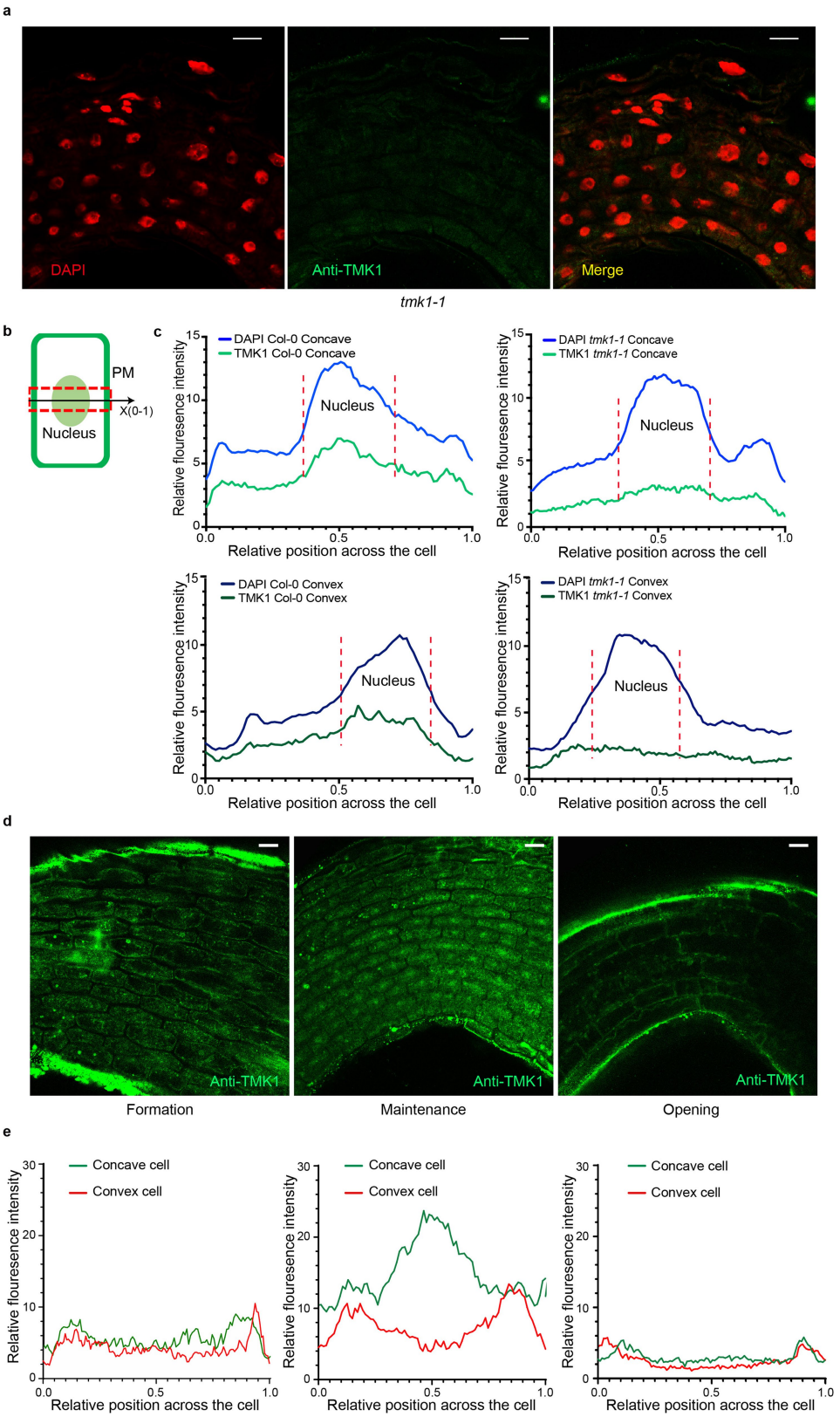

Extended Data Fig. 3 | See next page for caption.

Extended Data Fig. 3 | Immunolocalization of TMK1 during apical-hook development. a, Immunolocalization of TMK1 protein and DAPI staining at the apical-hook maintenance stage in *tmk1-1* mutants. The immunostaining was performed using same condition as those in Fig. 1d. Scale bars, 20 μm. Three biological repeats. **b**, Schematic showing the region (dashed frame) across the cells used for the quantification of fluorescence signal. **c**, Quantification of the relative intensity of $TMK1_{C\text{-}terminus}$ immunofluorescence and DAPI across a representative cell from both concave (top) or convex (bottom) sides of apical hook in Col-0 (left) and the *tmk1-1* (right) mutant. Dashed lines define the nucleus by the enriched DAPI signal. Fluorescence intensity was calculated using ImageJ, and normalized by the maximum intensity at 255. The position across the cell was normalized as 0–1, as shown in **b**. Twenty cells from four biologically independent seedlings showed a similar pattern. **d**, Representative images of immunolocalization of TMK1 in the apical hook at three different stages (formation, maintenance and opening). Scale bars, 20 μm. Three biological repeats. **e**, Quantification of the relative intensity of $TMK1_{C\text{-}terminus}$ immunofluorescence and DAPI across representative cells from concave and convex sides of the apical hook, at three different stages. Normalization was done as in **c**. Twenty cells from four biologically independent seedlings showed a similar pattern.

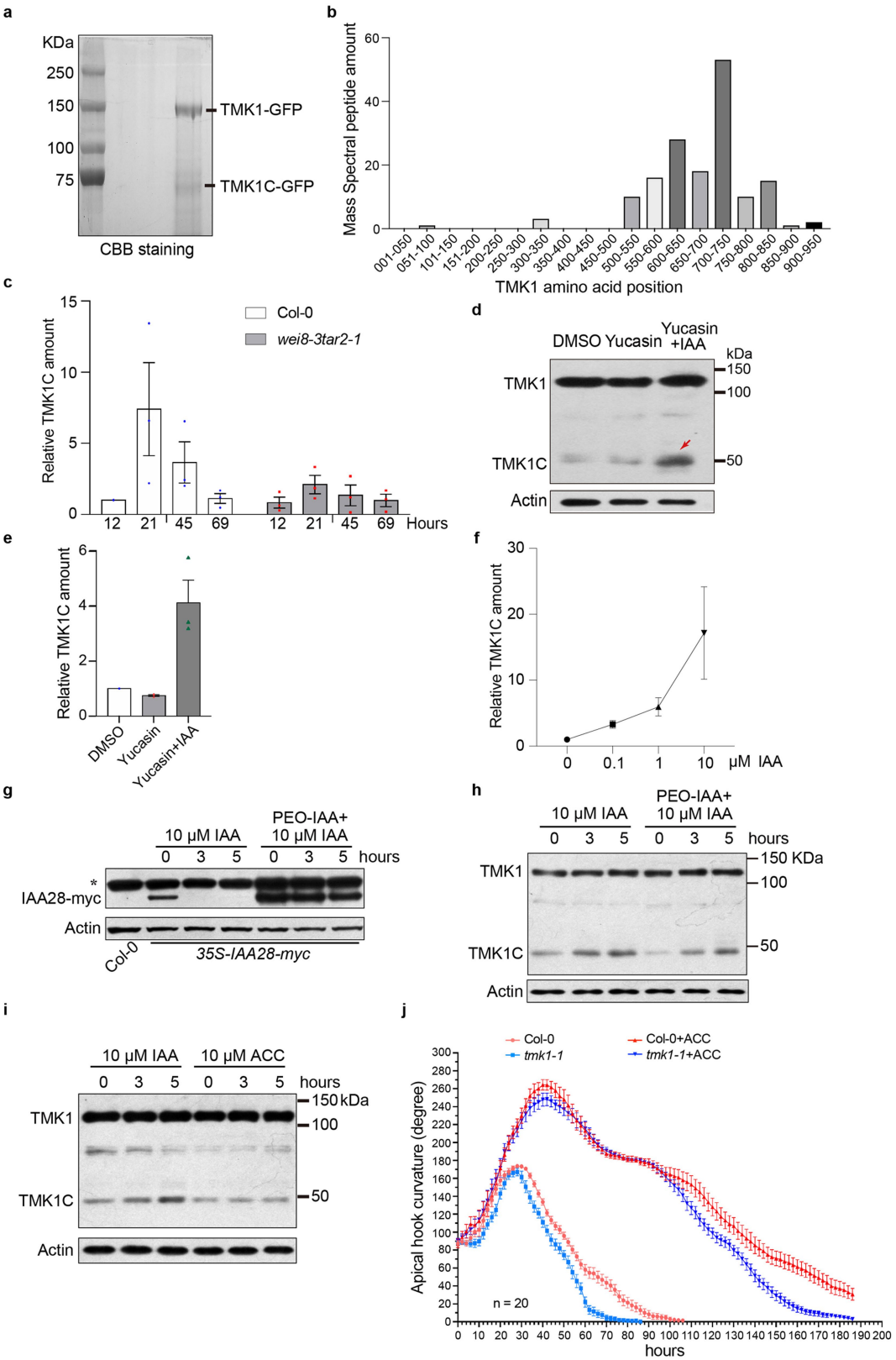

Extended Data Fig. 4 | See next page for caption.

Extended Data Fig. 4 | Cleavage of TMK1$_{C\text{-terminus}}$ is independent of both the auxin–TIR1 and the ethylene pathways. a, Identification of TMK1 C terminus. Full-length TMK1 and TMK1$_{C\text{-terminus}}$ were immunoprecipitated from *gTMK1-GFP* seedlings and separated by SDS–PAGE. Three biological repeats were performed with similar results. **b**, Mass spectrometry analysis of the TMK1$_{C\text{-terminus}}$ band. Results are displayed as spectral counts of the peptide fragment (*y* axis) along the TMK1 amino acid position (*x* axis). **c**, Quantification of western blotting results shown in Fig. 1f. **d**, Treatment with yucasin and auxin affects TMK1 cleavage. **e**, Quantification of western blotting results shown in **d**. **f**, Quantification of western blotting results shown in Fig. 1g. $n = 3$. **g**, The effect of treatment with PEO-IAA was tested by the inhibition of auxin-mediated IAA28 degradation by *35S-IAA28-MYC* transgenic line. Col-0 was used as a negative control; the asterisk indicates a non-specific band. **h**, The effect of treatment with PEO-IAA on auxin-mediated TMK1 cleavage. Three biological repeats. **i**, The effect on TMK1 cleavage of treatment with 10 μM ACC for a short period. Three biological repeats. For **d**, **g**–**i**, the same membrane was stripped and blotted with anti-actin antibodies as a loading control. **j**, Apical-hook development in the presence and absence of ACC in both Col-0 and *tmk1-1* plants. $n = 20$. Data are mean ± s.e.m.; dots show data distribution. *n* denotes the number of biologically independent seedlings.

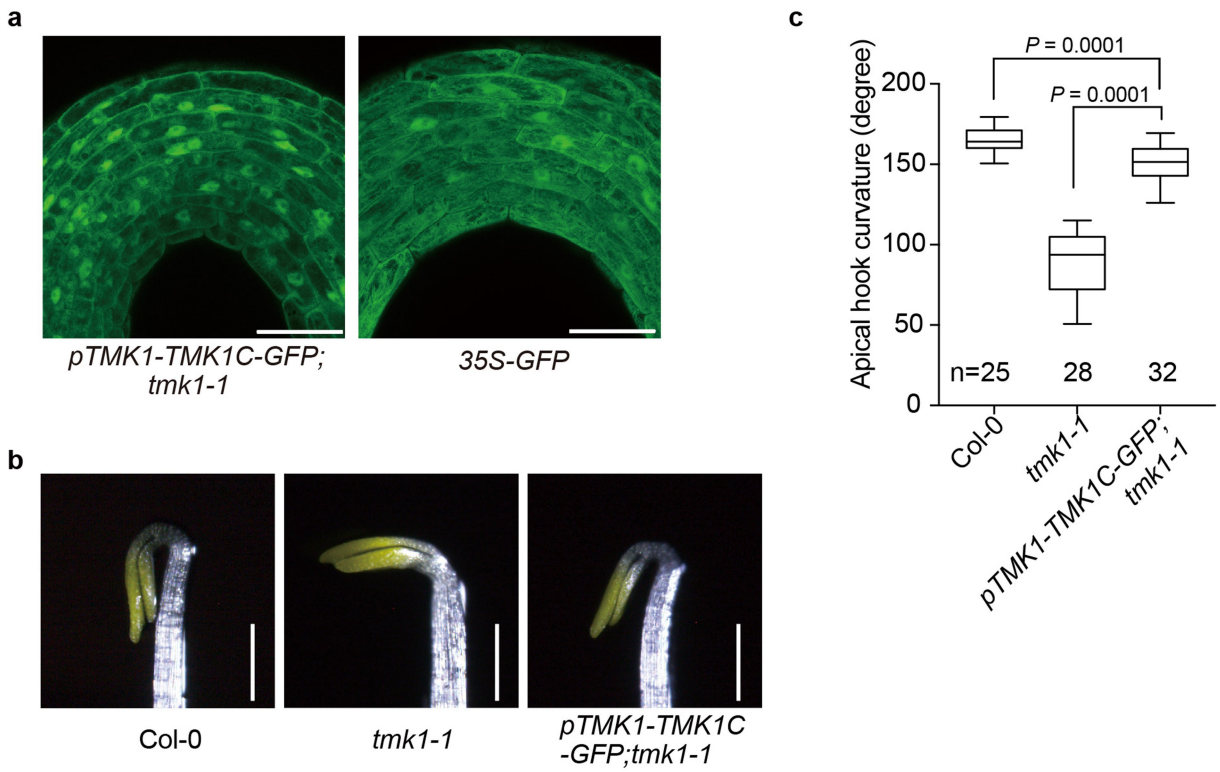

Extended Data Fig. 5 | TMK1$_{C\text{-terminus}}$ partially rescues the phenotype associated with the *tmk1* mutant. a, Representative images of TMK1$_{C\text{-terminus}}$–GFP localization in epidermal cells of the apical hook in the *pTMK1-TMK1$_{C\text{-terminus}}$-GFP* transgenic line. The *35S-GFP* line was used as a control. Scale bars, 50 μm. Three individual lines showed a similar pattern. **b**, Representative images of *pTMK1-TMK1$_{C\text{-terminus}}$-GFP* plants, which partially complemented the *tmk1-1* phenotype at 45 h after germination. Three out of three T3 individual homozygous lines showed similar phenotypes. Scale bars, 500 μm. **c**, Quantification of apical-hook curvature in **b**. Measurements displayed as box plots, showing the first and third quartiles, split by the median and extended to minimum and maximum values. Col-0 ($n = 25$), *tmk1-1* ($n = 28$), *pTMK1-TMK1$_{C\text{-terminus}}$-GFP;tmk1-1* ($n = 32$). *n* denotes the number of biologically independent seedlings. Two-sided *t*-test.

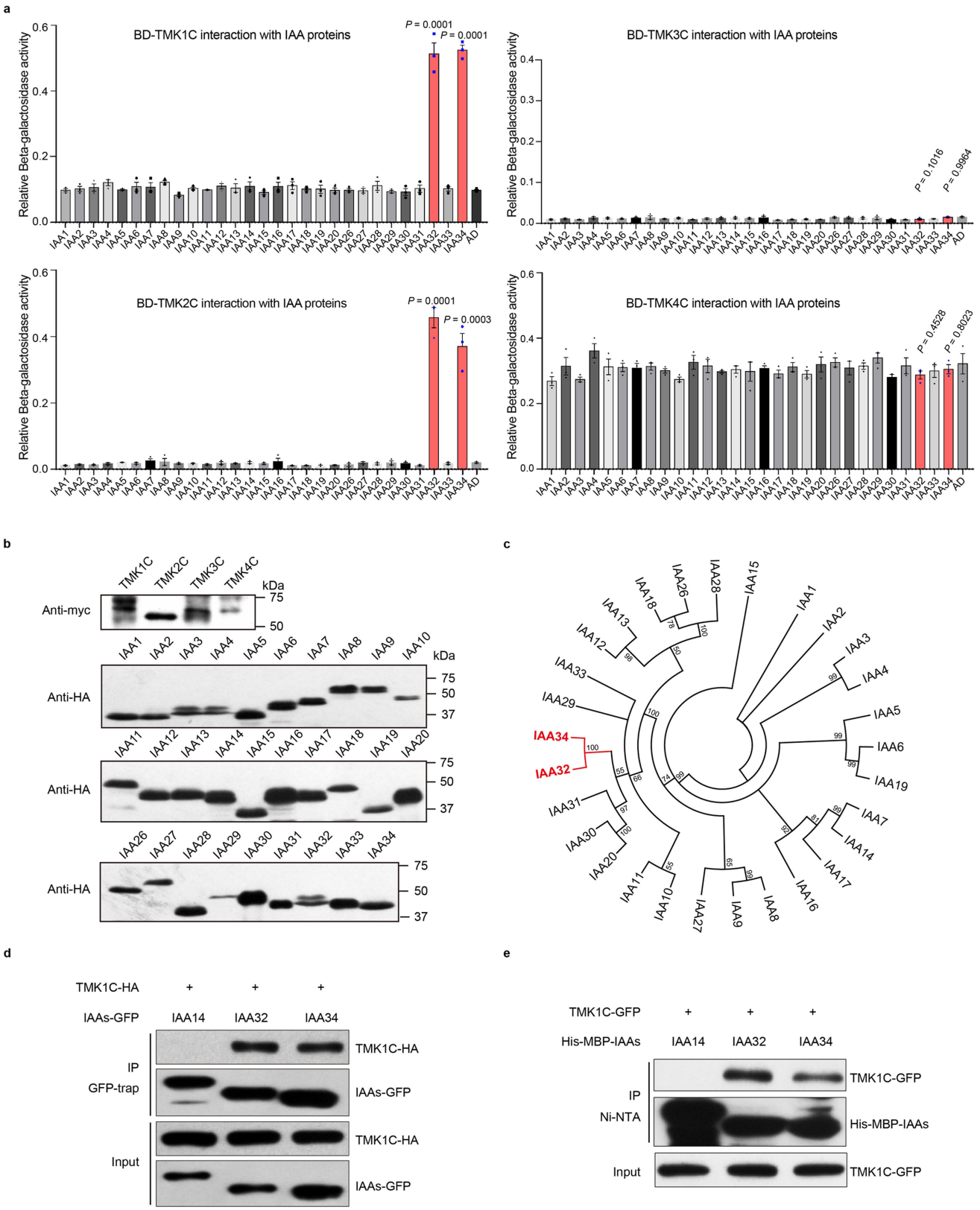

Extended Data Fig. 6 | See next page for caption.

Extended Data Fig. 6 | TMK1$_{C\text{-}terminus}$ specifically interacts with IAA32 and IAA34. a, Quantification of protein–protein interactions between TMK family members and IAA family members in yeast, by β-galactosidase assay. Three biologically independent experiments were performed for quantification. Data are mean ± s.e.m., one-way ANOVA with Dunnett's multiple-comparisons test compared to activation domain. Dots show data distribution. **b**, Protein expression verification for yeast two-hybrid interactions by western blotting. Experiment was repeated twice with similar results. **c**, Bayesian phylogenetic tree of the 29 IAA proteins in *A. thaliana*. This phylogenetic tree was generated through Bayesian inference, using the JTT model with 100,000 generations. The posterior probabilities are indicated (in per cent) at the base of each bipartition. **d**, TMK1$_{C\text{-}terminus}$ interacts with IAA32 and IAA34 in protoplasts. 35S–IAA32–GFP, 35S–IAA34–GFP and 35S–TMK1$_{C\text{-}terminus}$–HA were co-expressed in *Arabidopsis* protoplasts for co-immunoprecipitation (IP). 35S–IAA14–GFP was used as a control. Three biological repeats with similar results. **e**, TMK1$_{C\text{-}terminus}$ interacts with IAA32 and IAA34, shown by in vitro pull-down assay. TMK1$_{C\text{-}terminus}$–GFP protein from *pTMK1-TMK1$_{C\text{-}terminus}$-GFP* transgenic plants was incubated with *E. coli*-purified IAA32 and IAA34 recombinant protein. IAA14 was used as a control. Three biological repeats with similar results.

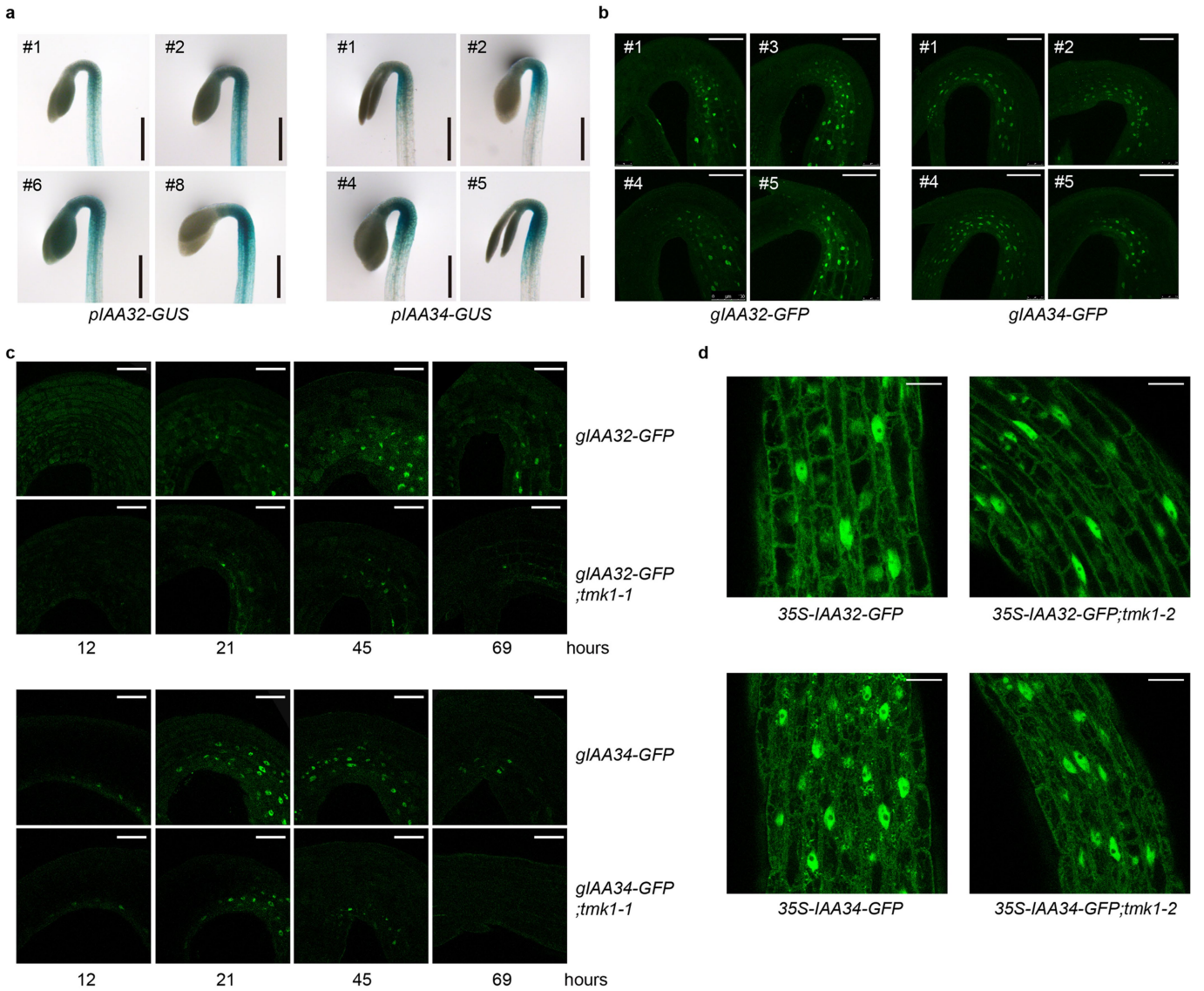

Extended Data Fig. 7 | IAA32 and IAA34 express in the apical-hook bending region, and localize in both the cytosol and nucleus. **a**, Expression patterns of *IAA32* and *IAA34* in three-day-old seedlings of *pIAA32-GUS* and *pIAA34-GUS* lines. Four independent T2 heterozygous plants are displayed. Scale bars, 500 μm. Representative of eight out of eight lines (*pIAA32-GUS*), or seven out of eight lines (*pIAA34-GUS*). **b**, Expression pattern of IAA32–GFP and IAA34–GFP proteins in three-day-old seedlings of *gIAA32-GFP* and *gIAA34-GFP* lines. Four independent T2 heterozygous plants are displayed. Scale bars, 50 μm. Representative of 11 out of 12 lines (*gIAA32-GFP*) or 9 out of 11 lines (*gIAA34-GFP*). **c**, Temporal and spatial expression patterns of IAA32 and IAA34 protein in both wild-type and *tmk1-1* plants during apical-hook development. Scale bars, 50 μm. Three individual lines of T3 homozygous plants showed a similar pattern. **d**, Representative images of subcellular localization of 35S–IAA32–GFP and 35S–IAA34–GFP at the apical hook of wild-type plants and *tmk1-2* mutant. Scale bars, 25 μm. Three individual lines of T3 homozygous plants showed a similar subcellular localization pattern.

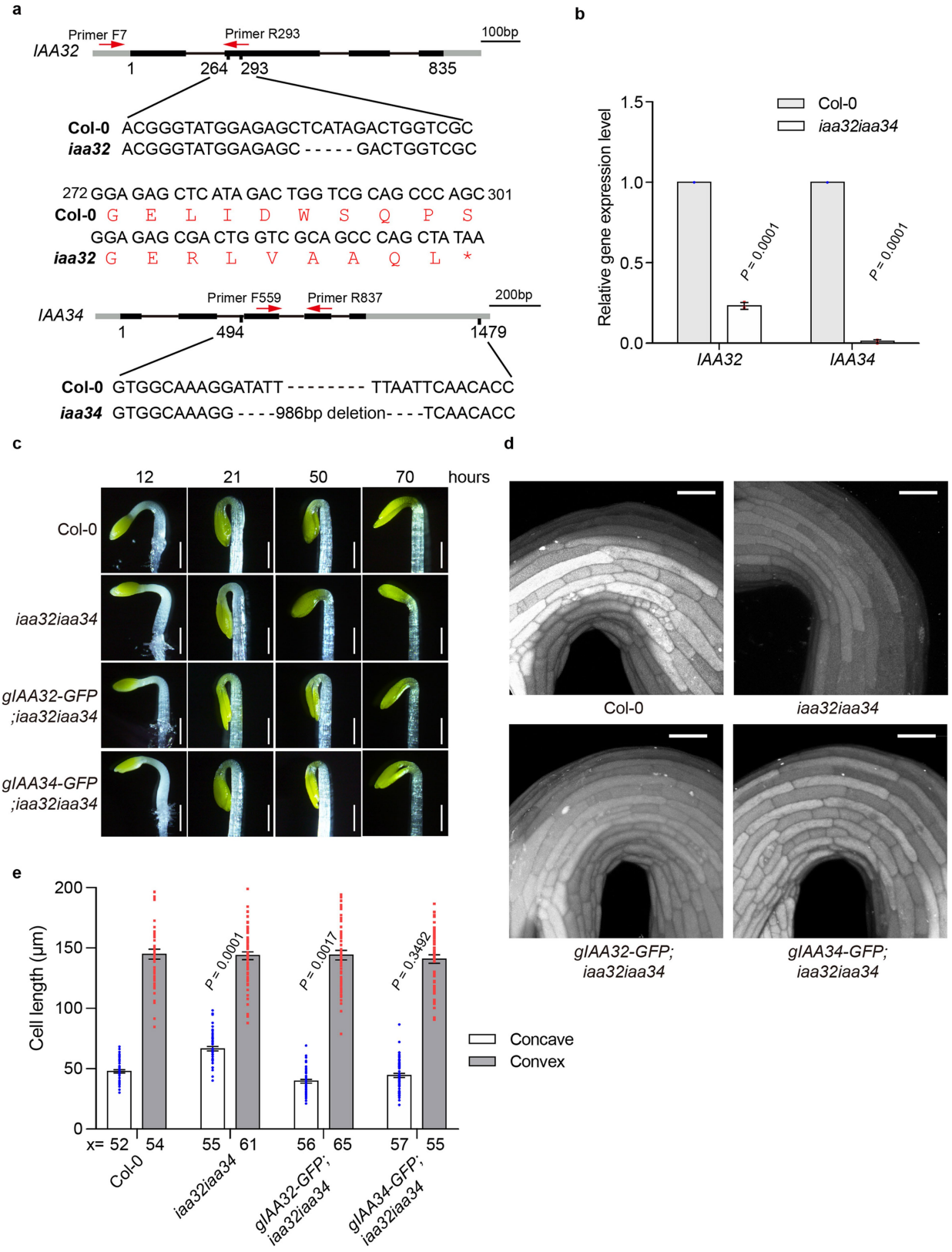

Extended Data Fig. 8 | See next page for caption.

Extended Data Fig. 8 | The *iaa32 iaa34* mutant shows cell-elongation defects at the apical hook. a, Schematic gene structure of *IAA32* and *IAA34*, with *iaa32* and *iaa34* mutants indicated. Lines represent introns; black and grey boxes represent exons and untranslated regions, respectively. Asterisk indicates the early stop codon in the *iaa32* mutant. Dashes indicate the deleted DNA base pairs. Arrows indicate primers that were used for quantitative PCR with reverse transcription analysis in **b**. Bar indicates the respective DNA lengths. **b**, Gene expression analysis of *IAA32* and *IAA34* transcripts in the *iaa32 iaa34* double mutant. Three biological repeats. Dots show data distribution. Two-sided *t*-test. Data are mean ± s.d. The expression levels were standardized as 1 in Col-0. *UBQ10* was used as an internal control. **c**, Representative images of apical hooks in Col-0, *iaa32 iaa34*, complementing *gIAA32-GFP;iaa32 iaa34* and complementing *gIAA34-GFP;iaa32 iaa34* lines. The growth conditions are comparable to those of experiments shown in Extended Data Fig. 1h. Scale bar, 500 μm. **d**, Images of the apical-hook epidermal cell in Col-0, *iaa32 iaa34*, *gIAA32-GFP;iaa32 iaa34* and *gIAA34-GFP;iaa32 iaa34* lines. Scale bars, 50 μm. Three biological repeats were performed with similar results. **e**, Quantification of cell length at the concave and convex sides of the apical hook, shown in **d**. Number of biologically independent seedlings: Col-0, $n = 10$; *iaa32 iaa34*, $n = 12$; *gIAA32-GFP;iaa32 iaa34*, $n = 11$; *gIAA34-GFP;iaa32 iaa34*, $n = 10$. *x* denotes cell numbers. Dots show data distribution. Two-sided *t*-test. Data are mean ± s.e.m.

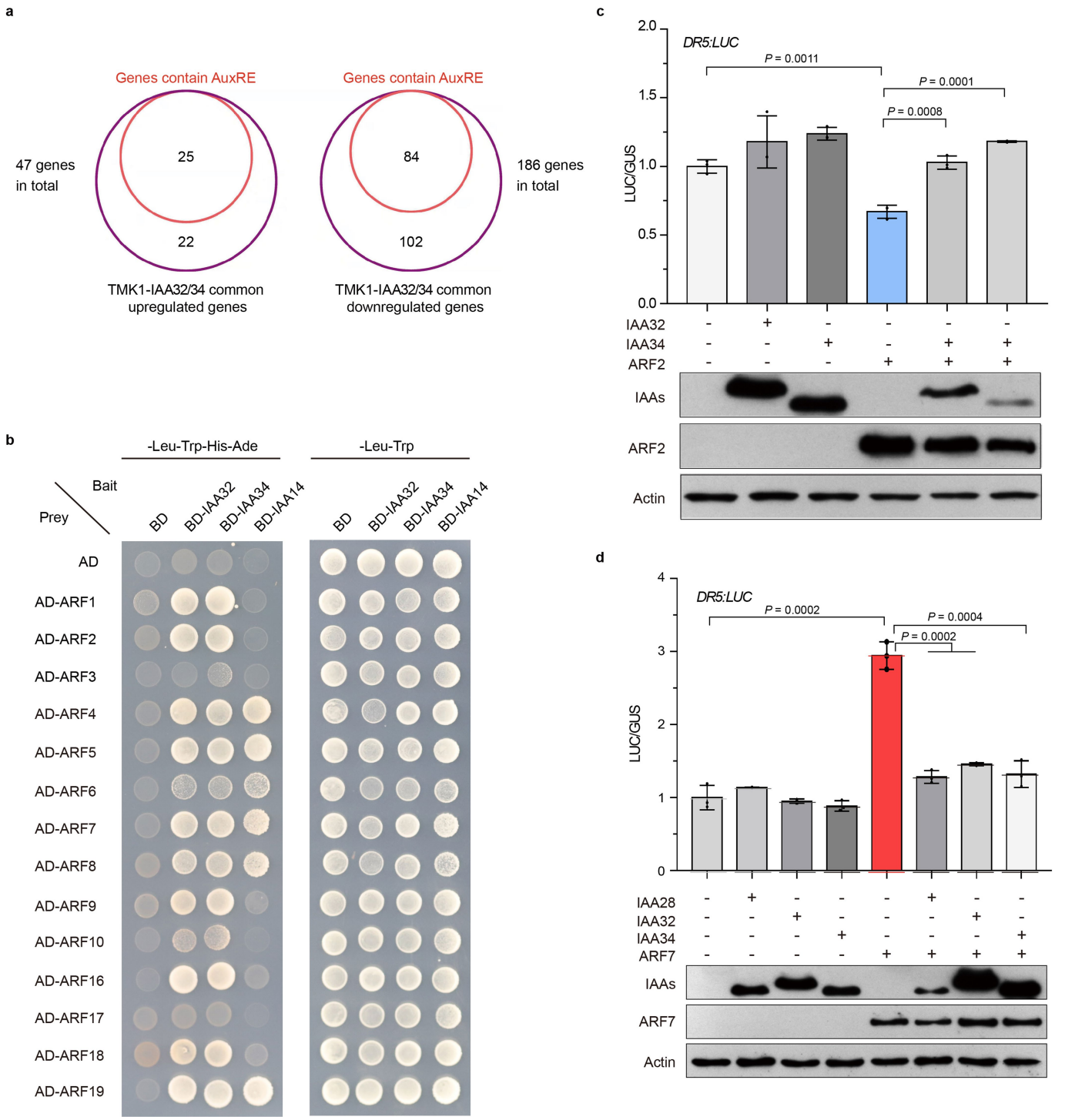

Extended Data Fig. 9 | IAA32 and IAA34 interact with ARFs, and suppress ARF activity. a, Auxin-response element (AuxRE) analyses in genes that are co-regulated by TMK1, IAA32 and IAA34. The auxin-response element motif (TGTCTC) within the 2-kb upstream promoter of differentially regulated genes was analysed. Twenty-five out of forty-seven genes that are upregulated by TMK1, IAA32 and IAA34 contained the auxin-response element; 84 out of 186 genes that are downregulated by TMK1, IAA32 and IAA34 contained the auxin-response element. Venn diagrams are used to present the comparison and overlaps of the gene lists. **b**, Protein–protein interactions between IAA proteins (IAA32, IAA34 and IAA14), and ARF family members in yeast two-hybrid analysis. Three biological repeats were performed with similar results. **c**, IAA32- and IAA34-inhibited ARF2 activity in *Arabidopsis* protoplasts. **d**, IAA32- and IAA34-inhibited ARF7 activity in *Arabidopsis* protoplasts. Top, relative luciferase (LUC) activity of DR5–LUC with co-expression of ARF and IAA proteins, as indicated. Bottom, protein expression by western blot. For **c**, **d**, the same membrane was stripped and blotted with anti-actin antibodies as a loading control. Luciferase activities were normalized by both GUS activity and the empty-vector control. $n = 3$ independent biological repeats. Two-sided t-test. Dots show data distribution, data are mean ± s.d.

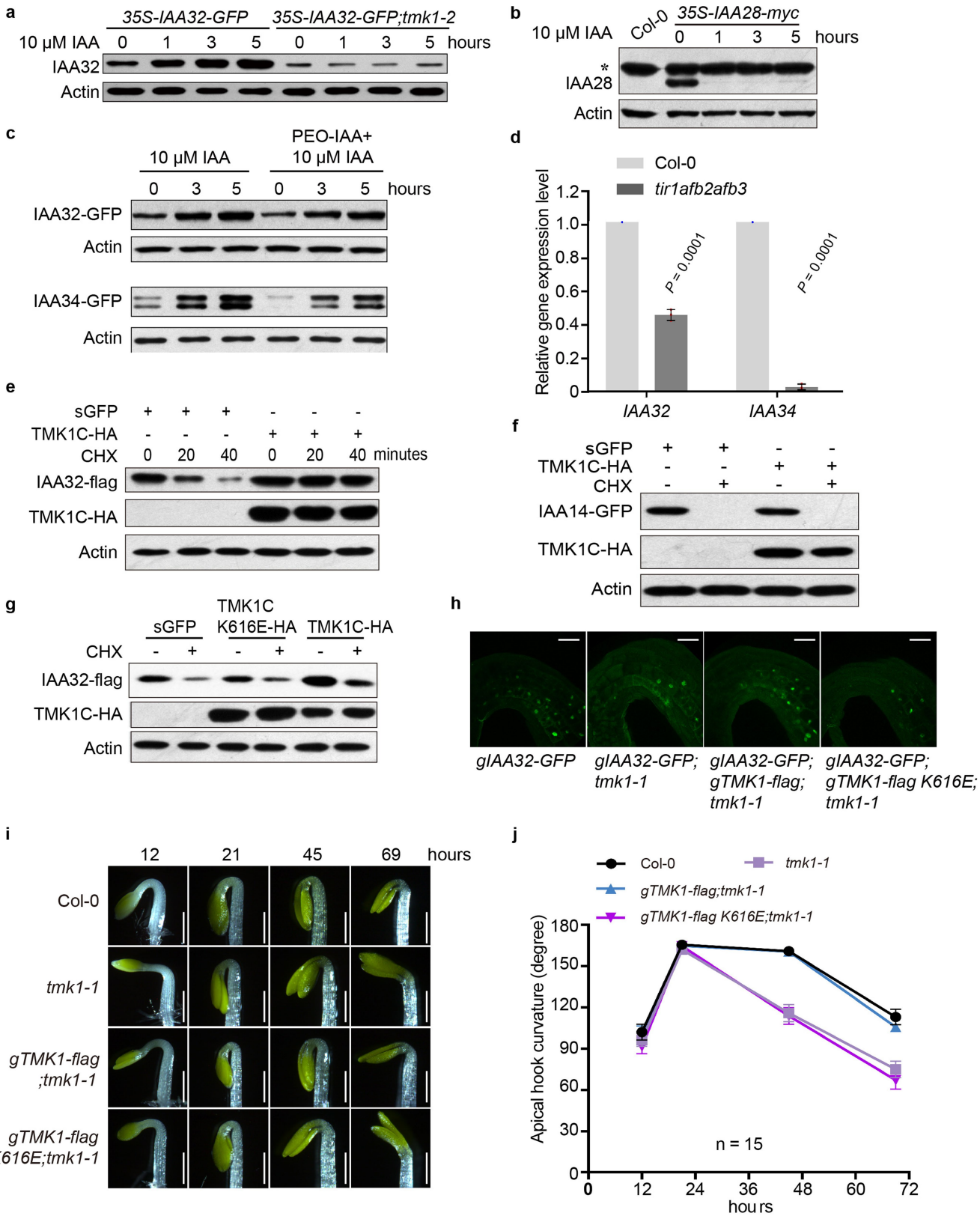

Extended Data Fig. 10 | See next page for caption.

Extended Data Fig. 10 | Transcriptional regulation of IAA32 and IAA34 depends on TIR1, but protein stability depends on the kinase activity of TMK1. a, Western blotting analysis of etiolated *35S-IAA32-GFP* line in either wild-type or *tmk1*, treated with auxin for indicated time points. Three biological repeats. **b**, Western blotting analysis of *35S-IAA28-MYC* line treated with auxin for indicated time points; asterisk indicates non-specific band. Three biological repeats. **c**, The TIR1 inhibitor PEO-IAA did not affect auxin-mediated accumulation of IAA32 and IAA34. Three biological repeats. **d**, Level of *IAA32* and *IAA34* transcription was downregulated in *tir1 afb2 afb3* mutant. Three biological repeats. Dots show data distribution. Two-sided *t*-test. Data are mean ± s.d. The expression level was standardized to 1 in wild-type seedlings. *UBQ10* was used as internal control. **e**, The protein stability of IAA32 with or without co-expression of 35S–$TMK1_{C\text{-}terminus}$–HA. CHX treatment for indicated time periods. 35S–sGFP was used as a control. Three biological repeats. **f**, Western blot of proteins in protoplasts co-transfected with HBT–$TMK1_{C\text{-}terminus}$–HA and HBT–IAA14–GFP. Three repeats showed similar results. **g**, The protein stability of IAA32 with or without co-expression of 35S–$TMK1_{C\text{-}terminus}$–HA. CHX treatment for indicated time periods. 35S–sGFP was used as a control. Three biological repeats. **h**, Confocal microscopy of IAA32–GFP protein in the apical hook of a *tmk1* mutant with *gTMK1-FLAG* or *gTMK1(K616E)-FLAG*. Scale bars, 50 μm. Three biological repeats. **i**, Representative images of apical hooks in Col-0, *tmk1-1*, g*TMK1-FLAG;tmk1-1* and g*TMK1(K616E)-FLAG;tmk1-1* at indicated time points after germination, Scale bars, 500 μm. Three independent repeats showed similar results. **j**, Quantification of apical-hook curvature at the time points corresponding to those shown in **i**. $n = 15$ biologically independent seedlings; data are mean ± s.e.m. For western blot images **a**–**c** and **g**, the same membrane was stripped and blotted with anti-actin antibodies as a loading control. For **f**, IAA14–GFP and $TMK1_{C\text{-}terminus}$–HA were run separately (with the same amount of protein per 10-μl sample) owing to the similar molecular mass of these two proteins. The same membrane of IAA14–GFP was stripped and blotted by anti-actin antibodies as a loading control.

nature research

Corresponding author(s): Tongda Xu

Reporting Summary

Nature Research wishes to improve the reproducibility of the work that we publish. This form provides structure for consistency and transparency in reporting. For further information on Nature Research policies, see Authors & Referees and the Editorial Policy Checklist.

Statistical parameters

When statistical analyses are reported, confirm that the following items are present in the relevant location (e.g. figure legend, table legend, main text, or Methods section).

n/a	Confirmed	
☐	☒	The exact sample size (*n*) for each experimental group/condition, given as a discrete number and unit of measurement
☐	☒	An indication of whether measurements were taken from distinct samples or whether the same sample was measured repeatedly
☐	☒	The statistical test(s) used AND whether they are one- or two-sided *Only common tests should be described solely by name; describe more complex techniques in the Methods section.*
☒	☐	A description of all covariates tested
☐	☒	A description of any assumptions or corrections, such as tests of normality and adjustment for multiple comparisons
☐	☒	A full description of the statistics including central tendency (e.g. means) or other basic estimates (e.g. regression coefficient) AND variation (e.g. standard deviation) or associated estimates of uncertainty (e.g. confidence intervals)
☐	☒	For null hypothesis testing, the test statistic (e.g. *F*, *t*, *r*) with confidence intervals, effect sizes, degrees of freedom and *P* value noted *Give P values as exact values whenever suitable.*
☐	☒	For Bayesian analysis, information on the choice of priors and Markov chain Monte Carlo settings
☒	☐	For hierarchical and complex designs, identification of the appropriate level for tests and full reporting of outcomes
☒	☐	Estimates of effect sizes (e.g. Cohen's *d*, Pearson's *r*), indicating how they were calculated
☐	☒	Clearly defined error bars *State explicitly what error bars represent (e.g. SD, SE, CI)*

Our web collection on statistics for biologists may be useful.

Software and code

Policy information about availability of computer code

Data collection	Proteomic data was collected by Orbitrap Fusion (Thermo Fisher Scientific, Watham, MA), by software Thermo Xcalibur 3.0.63. RNAseq data was collected by Illumina HiSeq2500, by software Real-Time Analysis (RTA) version 1.18.64.
Data analysis	Proteomic analysis: Mascot Daemon 2.5.0.100(64-bit) (Matrix Science, London, UK) RNAseq analysis: FastQC Version 0.11.5 Alignments: Geneious® 10.2.3 Statistical analysis: GraphPad Prism 7 Image analysis: ImageJ 1.52a

For manuscripts utilizing custom algorithms or software that are central to the research but not yet described in published literature, software must be made available to editors/reviewers upon request. We strongly encourage code deposition in a community repository (e.g. GitHub). See the Nature Research guidelines for submitting code & software for further information.

Data

Policy information about availability of data

All manuscripts must include a data availability statement. This statement should provide the following information, where applicable:

- Accession codes, unique identifiers, or web links for publicly available datasets
- A list of figures that have associated raw data
- A description of any restrictions on data availability

RNAseq raw data associated with Fig3d-f are available at the Gene Expression Omnibus under accession number: GSE111716.
Source Data (gels and graphs) for Fig1, 3, 4 and Extended Fig 1-6,8-10 are provided with manuscript.
The data supporting the findings in this study are available and described within the manuscript and its extended data.

Field-specific reporting

Please select the best fit for your research. If you are not sure, read the appropriate sections before making your selection.

☒ Life sciences ☐ Behavioural & social sciences

For a reference copy of the document with all sections, see nature.com/authors/policies/ReportingSummary-flat.pdf

Life sciences

Study design

All studies must disclose on these points even when the disclosure is negative.

Sample size	Sample size was determined by previous publications. These were clearly indicated in each figure legends, and methods.
Data exclusions	No data was excluded
Replication	All attempts of replication by different people within the group were successful; the key data were repeated by other group were also successful.
Randomization	The samples were picked to do biochemistry assay is randomized.
Blinding	The key phenotype analysis was confirmed by double blind. We did not do blinding assay to biochemistry data because the loading of gel need a known sample order.

Materials & experimental systems

Policy information about availability of materials

n/a	Involved in the study
☐	☒ Unique materials
☐	☒ Antibodies
☒	☐ Eukaryotic cell lines
☒	☐ Research animals
☒	☐ Human research participants

Unique materials

Obtaining unique materials	All unique materials used are readily available from the authors, and can be requested from corresponding author by txu002@ucr.edu

Antibodies

Antibodies used	Commercial antibodies used: α-GFP (B-2, sc-9996, Santa Cruz, 1:2000 dilution), α-myc(myc epitope tag in pGBKT7 for Yeast two-hybrid assay) (100029-MM08, Sino Biological, 1:2000 dilution), α-HA-HRP (HA epitope tag in pGADT7 for Yeast two-hybrid assay) (HA-7, #H6533, Sigma, 1:2000 dilution), α-flag (# M20008L , Abmart, 1:2000 dilution), α-Actin (# M20009L , Abmart, 1:2000 dilution), α-HA (#M20003, Abmart, 1:2000 dilution), α-myc (# M20002L , Abmart, 1:2000 dilution), α-His(Abmart# M30111L, 1:2000 dilution), α-myc (Roche#11667149001, LOT: 10653800, 1:2000 dilution). Dylight488 Goat anti Rabbit IgG(Invitrogen, Cat. 35553,1:1000 dilution). Expect α-HA-HRP, other primary antibodies were detected using Goat Anti-Mouse IgG (H+L)-HRP Conjugate (#1721011, Bio-Rad). α-TMK1C was produced by ABclonal Biotechnology and used 1:2000 dilution for Western blot; 1:500 dilution for immunostaining. α-TMK1C primary antibodies were detected using Goat Anti-Rabbit IgG (H + L)-HRP Conjugate.(#1706515, Bio-Rad)
Validation	Validation statements of commercial primary antibodies are available from manufacturers: α-GFP-HRP(https://

datasheets.scbt.com/sc-9996.pdf),α-myc(myc epitope tag in pGBKT7 for Yeast two-hybrid assay) (http://www.sinobiologicalcdn.com/reagent/100029-MM08.pdf), α-HA-HRP(HA epitope tag in pGADT7 for Yeast two-hybrid assay), α-flag(www.ab-mart.com.cn/upload/20170614093631xz.pdf), α-Actin(www.ab-mart.com.cn/upload/20170614135558xz.pdf), α-HA (http://www.ab-mart.com.cn/upload/20170614093540xz.pdf), α-myc(http://www.ab-mart.com.cn/upload/20170614093526xz.pdf), α-His(http://www.ab-mart.com.cn/upload/20170614093741xz.pdf), α-myc (https://pim-eservices.roche.com/DownloadDocument/SDS/DE/en/11667149001). Dylight488 Goat anti Rabbit IgG, (https://www.thermofisher.com/order/genome-database/generatePdf?productName=Rabbit IgG (H+L) Cross-Adsorbed&assayType=PRANT&detailed=true&productId=35553)
α-TMK1C was validated by western blot and immunostaining respectively in the tmk1 mutant (Extended data 2a, 3a)

Method-specific reporting

n/a	Involved in the study
☒	☐ ChIP-seq
☒	☐ Flow cytometry
☒	☐ Magnetic resonance imaging